

## Topical Review

# Advanced defect spectroscopy in wide-bandgap semiconductors: review and recent results

Manuel Fregolent<sup>1,\*</sup>, Francesco Piva<sup>1,\*</sup>, Matteo Buffolo<sup>1,4</sup>, Carlo De Santi<sup>1</sup>, Andrea Cester<sup>1</sup>, Masataka Higashiwaki<sup>2,3</sup>, Gaudenzio Meneghesso<sup>1</sup>, Enrico Zanoni<sup>1</sup> and Matteo Meneghini<sup>1,4</sup>

<sup>1</sup> Department of Information Engineering, University of Padova, Padova, Italy

<sup>2</sup> Department of Physics and Electronics, Osaka Metropolitan University, Osaka, Japan

<sup>3</sup> National Institute of Information and Communications Technology, Tokyo, Japan

<sup>4</sup> Department of Physics and Astronomy, University of Padova, Padova, Italy

E-mail: [manuel.fregolent@unipd.it](mailto:manuel.fregolent@unipd.it) and [francesco.piva@unipd.it](mailto:francesco.piva@unipd.it)

Received 31 January 2024, revised 21 April 2024

Accepted for publication 25 June 2024

Published 8 August 2024



## Abstract

The study of deep-level defects in semiconductors has always played a strategic role in the development of electronic and optoelectronic devices. Deep levels have a strong impact on many of the device properties, including efficiency, stability, and reliability, because they can drive several physical processes. Despite the advancements in crystal growth, wide- and ultrawide-bandgap semiconductors (such as gallium nitride and gallium oxide) are still strongly affected by the formation of defects that, in general, can act as carrier traps or generation-recombination centers (G-R). Conventional techniques used for deep-level analysis in silicon need to be adapted for identifying and characterizing defects in wide-bandgap materials. This topical review paper presents an overview of reviews of the theory of deep levels in semiconductors; in addition, we present a review and original results on the application, limits, and perspectives of two widely adopted common deep-level detection techniques, namely capacitance deep-level transient spectroscopy and deep-level optical spectroscopy, with specific focus on wide-bandgap semiconductors. Finally, the most common traps of GaN and  $\beta\text{-Ga}_2\text{O}_3$  are reviewed.

Keywords: deep levels, wide-bandgap semiconductors, deep-level transient spectroscopy, deep-level optical spectroscopy, gallium nitride, gallium oxide

\* Authors to whom any correspondence should be addressed.



Original content from this work may be used under the terms of the [Creative Commons Attribution 4.0 licence](#). Any further distribution of this work must maintain attribution to the author(s) and the title of the work, journal citation and DOI.

## 1. Introduction

Since the beginning of semiconductor science, the study of semiconductor defects has been fundamental to our understanding of device physics due to the strong impact they have on the electrical and optical properties. While controlled defect formation has reached an excellent level of maturity in traditional semiconductors such as Si and GaAs, this is not the case in wide-bandgap semiconductors, where the concentration of deep levels is significant and still strongly impacts the performance of the devices. In fact, deep levels are responsible for several physical phenomena, including carrier trapping, which leads to parametric instability [1–5] and degradation of the dynamic performance [6–9]; they can act as recombination centers [10, 11], thus contributing to a decrease in the internal quantum efficiency of light emitters [12–15], a decrease in the carrier lifetime [16], and limited spectral purity of optoelectronic devices [17–20]. In addition, trap states can assist tunneling processes, which have detrimental effects on the reliability of several devices, including high electron mobility transistors (HEMTs) [21–23] and light-emitting diodes (LEDs) [24–27], and promote leakage current [22, 28].

For these reasons, the analysis of defects has always been of great interest, and several techniques have been developed to detect traps by means of electrical techniques (capacitance deep-level transient spectroscopy (C-DLTS) [29], thermal admittance spectroscopy (TAS) [30]), optical techniques (capacitance deep-level optical spectroscopy (DLOS) [31], and photoluminescence), and others, such as electron paramagnetic resonance [32, 33]. We note here that C-DLTS and DLOS, which have been developed for narrow-gap materials, have some limitations when applied to wide-bandgap semiconductors: specific adaptation and a review of the related theoretical fundaments are required to fully exploit the potential of such techniques.

This paper intends to address this issue and review the use of C-DLTS and DLOS with specific reference to wide-bandgap semiconductors; in addition, we present an overview of the properties and models for deep traps in two relevant materials: GaN and  $\beta\text{-Ga}_2\text{O}_3$ .

The paper is organized as follows. Section 2 describes the main properties and applications of wide-bandgap semiconductors, with an overview focused on gallium nitride and gallium oxide devices. Then, section 3 discusses the main features of deep levels in semiconductor materials, and describes the two main approaches to understand the deep-level physics: (3.1) the traditional Shockley–Read–Hall (SRH) model and (3.2) the multi-phonon emission (MPE) framework, analyzed through the *generalized configuration coordinate diagram* (GCCD). Then, section 4 reports a review of the two main spectroscopic techniques for the electrical characterization of deep levels: (4.1) DLTS and (4.2) DLOS. A brief review of the techniques employed for deep-level detection in transistors is presented in (4.3). Section 5 presents a case study on the analysis of deep levels by DLOS in N-implanted  $\beta\text{-Ga}_2\text{O}_3$  Schottky barrier diodes (SBDs). Finally, in sections 6 and 7, the most common defects for  $\beta\text{-Ga}_2\text{O}_3$  and GaN are revised.

**Table 1.** Fundamental physical parameters of the most established wide-bandgap semiconductors.

	Si	SiC	GaN	$\beta\text{-Ga}_2\text{O}_3$
$E_G$ [eV]	1.12	3.3	3.4 <sup>a</sup>	4.8 <sup>a</sup>
$E_C$ [MV cm <sup>-1</sup> ]	0.3	2.6	3.3	6–8
$\mu_n$ [cm <sup>2</sup> V <sup>-1</sup> s <sup>-1</sup> ]	1400	1000	1200	450
$\mu_p$ [cm <sup>2</sup> V <sup>-1</sup> s <sup>-1</sup> ]	450	90–120	120	—
$k$ [W m <sup>-1</sup> K <sup>-1</sup> ]	149	340	130	10–30
Normalized Baliga Figure of Merit	1	340	870	2870

<sup>a</sup> Direct bandgap.

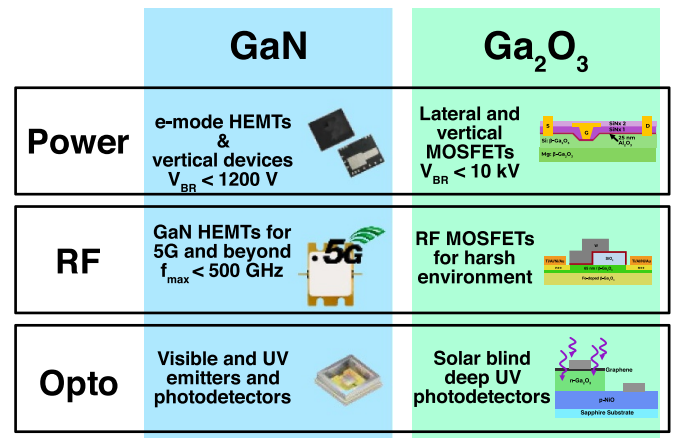


**Figure 1.** Perspective power, RF, and optoelectronics applications of wide-bandgap semiconductors GaN and  $\beta\text{-Ga}_2\text{O}_3$  [50, 62, 63].

## 2. Wide-bandgap semiconductors and applications

Among the wide-bandgap semiconductors, gallium nitride (GaN) and gallium oxide ( $\text{Ga}_2\text{O}_3$ ) are attracting most of the attention of the electron device community due to their excellent material properties (table 1) and wide range of applications, which include power transistors and rectifiers, RF amplifiers, light emitters, and detectors (figure 1).

Originally, gallium nitride technology was studied to cover the blue gap in solid-state light emitters [34]. Thanks to the excellent optical properties and the simple bandgap engineering with aluminum and indium alloying, GaN-based LEDs can cover the light spectrum from UV to IR [35–38].

As a consequence of the presence of spontaneous and piezoelectric polarization charges, the large bandgap, and the high critical electric field, GaN enabled the design of HEMTs based on the AlGaN/GaN heterojunction, which are now becoming excellent candidates for RF amplifiers for 5G and beyond [39–41], and power devices with a operating voltage of 650 V and more [42]. In addition, vertical power transistors targeting 1200 V and above are under study [43–45].

The development of gallium oxide as a possible candidate for the next generation of power devices started in 2012, when Higashiwaki *et al* demonstrated the first  $\beta\text{-Ga}_2\text{O}_3$  lateral transistor with an impressive breakdown voltage above 250 V [46]. Thanks to the ‘ultrawide’ bandgap of 4.85 eV

and the large critical electric field, the main target for gallium oxide was power transistors with operating voltage in the order of 10 kV [47, 48]; currently, both lateral [49–52] and vertical [53–55] transistors are under study, with performances that are rapidly approaching that of SiC and GaN devices. Furthermore, thanks to the good electron mobility and the high saturation velocity of  $2 \times 10^6 \text{ cm s}^{-1}$ , RF transistors for harsh environments are also under study [56]. Finally, the ultrawide bandgap of gallium oxide gives a low absorption coefficient for visible light, thus enabling the design of solar blind photodetectors for communication and detection of the deep UV spectrum [57, 58]. Among the several different polytypes ( $\alpha-$ ,  $\beta-$ ,  $\gamma-$ ,  $\delta-$ ,  $\kappa-$ ) [59, 60], the monoclinic ( $\beta-$ ) phase is the most studied because of its superior thermal stability up to 1700 °C [47, 61].

### 3. Deep levels in semiconductor materials

The electrical and optical properties of a semiconductor material are intimately connected with the crystal lattice and the periodic potential defined by the atomic bonds. In a real crystal, imperfections of the periodic lattice structure are unavoidable. These are mainly caused by *intrinsic* defects due to the absence of atoms (vacancies) and misplacement of the atoms in the matrix [64] (antisite, self-interstitial); alternatively, levels can be attributed to *extrinsic* causes, such as the incorporation of atomic impurities that ideally should not be present in the host matrix. In addition, based on their dimensionality, we can distinguish between point defects (0-dimensional), dislocations (1-D), plane (2-D), and volumetric (3-D) defects. The presence of any semiconductor defect locally modifies the potential of the crystal, eventually creating allowed energy levels between the conduction band minimum ( $E_C$ ) or valence band maximum ( $E_V$ ) that can be electrically and optically active. In general, levels that are thermally ionized at room temperature ( $|E_C, V \mp E_T| < 30 \text{ meV}$ ) are referred to as *shallow levels* (commonly associated with doping and compensation of free charge); otherwise, they are known as *deep levels*.

#### 3.1. Traditional SRH recombination model

Deep levels can in general behave as G-R or carrier traps. The interaction between free carriers and trap states was originally described by the SRH model [11, 65] (figure 2), which takes into consideration four possible processes: electron and hole capture (modeled by the coefficients  $c_n$ ,  $c_p$ ), representing the relaxation of each carrier from the conduction (or valence) band to the trap state, and electron or hole emission, respectively modeled by the coefficients  $e_n$ ,  $e_p$ , representing the promotion of the carrier to the respective band.

Trap states can be occupied either by an electron or a hole; therefore, the sum of the trapped electron and hole concentrations, respectively  $n_T$  and  $p_T$ , corresponds to the total defect concentration  $N_T = n_T + p_T$ . It follows that the trapping rates for electrons and holes are given by the rate equations [66]

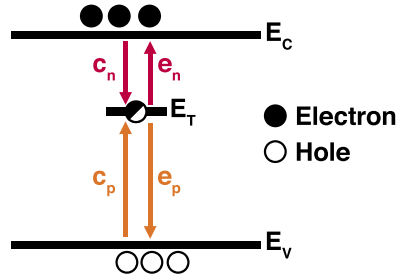


**Figure 2.** SRH model of the dynamic interaction between carriers and trap states. The four processes allowed by the model are described by the capture and emission coefficients  $c_n$ ,  $c_p$ ,  $e_n$ ,  $e_p$ .

$$\begin{aligned}\frac{dn_T}{dt} &= c_n n p_T - e_n n_T \\ \frac{dp_T}{dt} &= c_p p n_T - e_p p_T\end{aligned}\quad (1)$$

where  $n$  and  $p$  represent the free electron and hole concentrations in the conduction and valence bands. Since carriers are considered to randomly move at the thermal velocity  $v_{th,n/p}$ , to a first-order approximation the capture coefficients can be assumed to be equal to

$$\begin{aligned}c_n &= \sigma_n v_{th,n} \\ c_p &= \sigma_p v_{th,p}\end{aligned}\quad (2)$$

where  $\sigma_n$  and  $\sigma_p$  are the apparent capture cross-sections of the deep levels. Capture and emission transitions are typically mediated by the emission or absorption of phonons and photons, which contribute to the zero net energy and momentum budget. Although the SRH model correctly predicts many properties of semiconductor devices, and models in a reasonable way non-radiative recombination and other trapping processes, it fails to properly describe the interactions between carriers, photons, phonons, and trap levels in specific scenarios. For instance, the model does not consider the different relaxations of the lattice if the transition is phonon- or photon-mediated, the structural change of the defects upon changes of its charge state [67], and the presence of a capture barrier [68–70].

#### 3.2. GCCD and MPE

A more general description of the interaction between free carriers and deep levels in semiconductors is given by the GCCD (figure 3) [71]. In this kind of plot, the allowed electronic and vibrational states for the electrons (or holes) in the deep levels and in the conduction (or valence) band are represented as a function of the generalized coordinate, which basically defines the atom displacement in the crystal lattice. In fact, when an electron is trapped in a deep level, its wave function becomes strongly localized and the unbalanced charge state results in a distortion of the crystal, which needs to rearrange its structure to accommodate the new potential profile [72]. Since the characterization of the physical properties of a deep

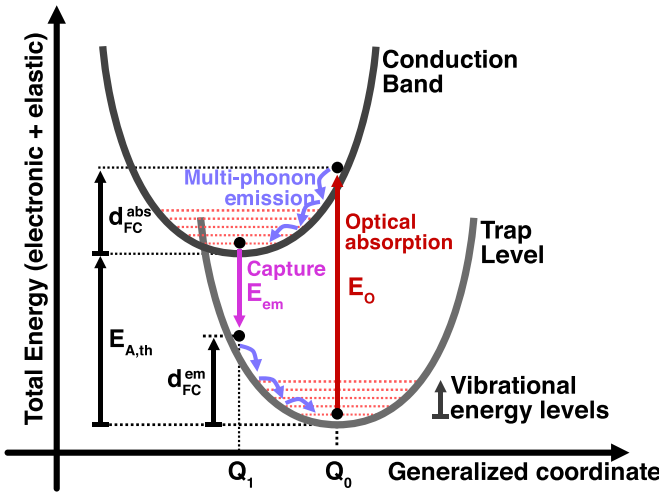


**Figure 3.** GCCD of a trap state. The arrows represent the processes of capture and emission via MPE and optical absorption.

level (e.g. activation energy or cross-section) typically proceeds through the evaluation of the effects of light (photons) and temperature (phonons) on the trapped states, this model is more suitable for investigating defect properties.

We will now consider the case of an electron trapped in a deep acceptor level. Its promotion to the conduction band can occur in two different ways: through the absorption of a photon or by thermal ionization. In the first case, according to the semiclassical Frank–Condon approximation, the nuclei of the lattice atoms are considered to be still during the transition, owing to the large relaxation time (compared to the time of the photon absorption process), and the electronic transition in the GCCD appears as vertical [73]. This requires an absorbed photon with energy above a certain threshold  $E_O^{abs}$ , which is a typical characteristic of the defect. Once the electron is promoted to the excited state (conduction band), the new electronic configuration forces the system to relax to a new equilibrium condition ( $Q_1$ ), by losing energy through MPE [72, 74].

The amount of energy emitted during relaxation is defined as the Frank–Condon shift  $d_{FC}^{abs}$ . Following the diagram in figure 3, the difference between the optical absorption energy  $E_O^{abs}$  and  $d_{FC}^{abs}$  represents the thermal activation (or binding) energy of the deep level  $E_{A, th}$ , i.e. the difference between the ground (vibronic) states of the trapped and excited states. We can therefore write that

$$E_O^{abs} - d_{FC}^{abs} = E_{A, th}. \quad (3)$$

On the other hand, when an electron is in the excited state, it can be trapped by the deep level with an optical or thermal transition. The first case is analogous to the optical absorption: the vertical transition results in an emission of a photon followed by MPE for the relaxation to equilibrium of the trapped state [70].

Let us now consider the non-radiative capture of an electron by a deep level. Generally speaking, since the GCCD parabolas associated with the deep level are misaligned

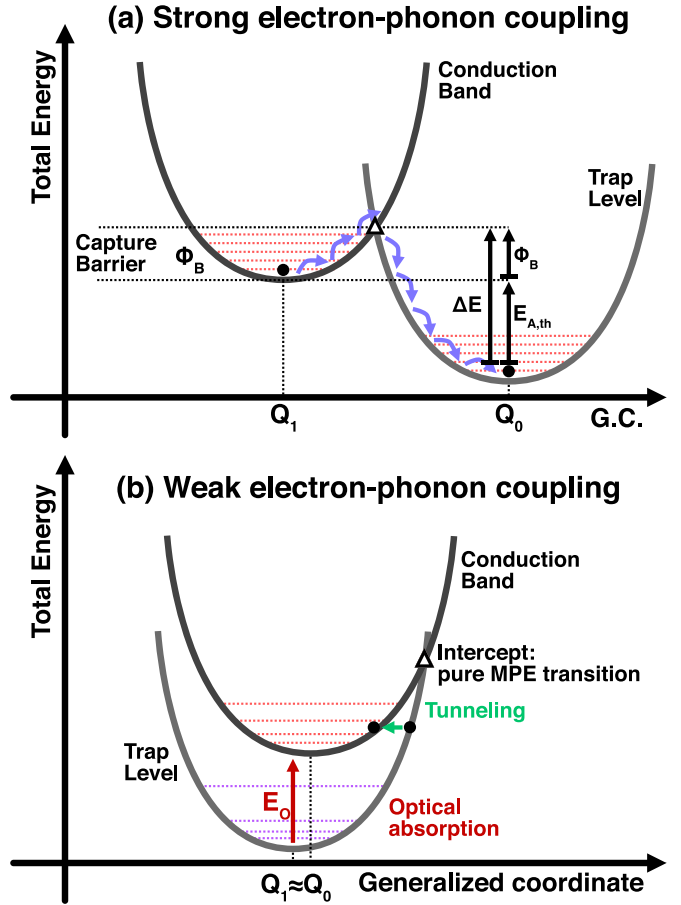


**Figure 4.** (a) GCCD for a non-radiative capture of a deep level with a strong electron–phonon coupling that presents a capture barrier  $\Phi_B$ . Before being trapped in the deep level, the electrons must gain a certain energy to overcome the capture barrier, thus introducing an additional energy term in the non-radiative capture process. (b) GCCD for generic capture and emission of carriers in the case of weak electron–phonon coupling [75].

(figure 4(a)), the electrons have to gain a certain amount of thermal energy (equal to the difference between the equilibrium energy in the excited state and the intersection between the two parabolas) before thermalizing in the trap state through MPE. The height of the capture barrier  $\Phi_B$  depends on the misalignment between the two GCCDs, and can assume a range of different values, from few meV to the eV range (see section 3 for more details); in most cases this barrier can be neglected, since its height is comparable to the thermal energy of the electrons.

From a first-order perspective, the degree of interaction between the trapped electrons and phonons can be represented by the Huang–Rhys factor  $S$ , which in principle counts the mean number of phonons emitted during absorption or emission [76]:

$$S = \frac{d_{FC}}{\hbar\omega_0}, \quad (4)$$

where  $\hbar\omega_0$  is the average phonon energy. Usually, weak electron–phonon interactions are considered for  $S < 1$ , and strong interactions for  $S \gg 1$ .

For weak electron–phonon interaction, the two parabolas that represent the ground (i.e. trapped) and excited states are almost aligned to one another ( $Q_0 \approx Q_1$ ). Therefore, the Frank–Condon shift for the absorption and emission process is  $d_{FC}^{abs} \approx d_{FC}^{emi} \approx 0$ . According to the Huang–Rhys model [76] the two parabolas are identical, therefore the crossover point at which a pure transition by MPE can happen has a high energy, leading to a low transition probability (figure 4(b)). Nevertheless, since the two levels are closely spaced in the GCCD, the transition can be mediated by the tunneling process at an energy that maximizes both the overlap between the available vibrational states and the tunneling probability.

#### 4. Techniques for defect spectroscopy

The detection and characterization of deep levels in semiconductors requires experimental techniques capable of obtaining all the important defect parameters, such as the defect concentration  $N_T$ , the thermal or optical ionization energy, the apparent capture cross-section and its temperature dependence, and their spatial distribution. To characterize charge trapping and detrapping processes, transient capacitance measurements on simple test structures, Schottky or  $p$ – $n$  diodes, are typically employed to quantitatively assess the aforementioned defect properties. In the following, we will discuss the two most common techniques for defect spectroscopy: C-DLTS and DLOS.

##### 4.1. C-DLTS

C-DLTS is a technique originally proposed by Lang in 1974 that is based on monitoring the temperature dependence of the capacitance transient associated with charge emission from deep levels previously filled with an appropriate voltage pulse [29]. A typical measurement procedure for a Schottky junction is shown in figure 5.

Let us first consider an SBD biased at a certain voltage  $V_m$ . Then, the junction is biased at the filling voltage  $V_F > V_m$  for a filling pulse  $t_f$ ; in this time frame the space charge region (SCR) shrinks, and the previously ionized defects at the edge of the SCR are filled by the relaxation of the electrons from the conduction band. After that, the junction is biased again at the measurement voltage  $V_m$ , and the electrons are thermally emitted to the conduction band, thus resulting in a variation of the fixed charge density, which ultimately leads to a variation of the junction capacitance. The emission rate  $e_n$  for each defect has an exponential dependence on the temperature:

$$e_n = \tau_n^{-1} = \frac{\sigma_n v_{th} N_C}{g} \exp\left(-\frac{q(E_C - E_T)}{k_B T}\right), \quad (5)$$

where  $\sigma_n$  is the apparent capture cross-section of the defect,  $v_{th} = \sqrt{\frac{3k_B T}{m_e^*}}$  is the thermal velocity of the electrons,  $N_C$  is the effective number of states in the conduction band,  $g$  is the degeneracy factor,  $E_C - E_T \triangleq E_A$  is the activation energy of the deep level,  $q$  is the electron charge,  $k_B$  is Boltzmann's constant,  $T$  is the absolute temperature, and  $m_e^*$  is the electron effective mass. Considering that during the measurement

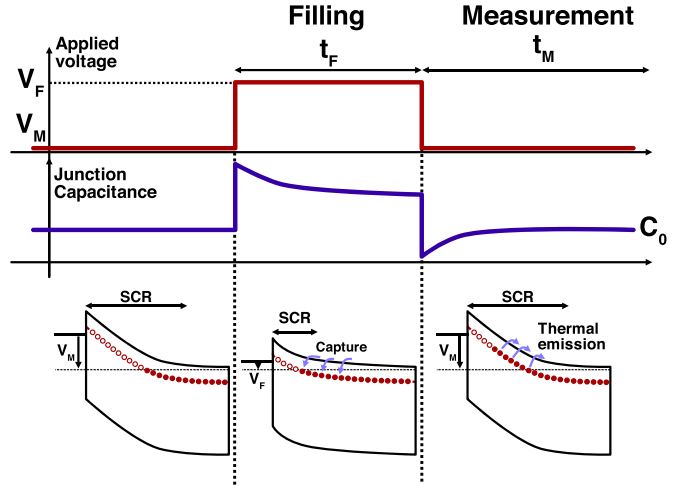


**Figure 5.** Typical measurement sequence of the C-DLTS technique.

phase the carrier capture is negligible with respect to the carrier emission, the solution of equation (1) is

$$n_T(t) = N_T \left[ 1 - \exp\left(-\frac{t}{\tau_n}\right) \right]. \quad (6)$$

Traditionally, the results of this experiment are represented with the so-called *rate window plot*, obtained with the double boxcar method [29], in which the C-DLTS signal  $S(T)$  is plotted as a function of the temperature as

$$S(T) = C(t_1) - C(t_2), \quad t_1 > t_2 \quad (7)$$

where  $C(t_i)$  is the junction capacitance and  $R = (t_1 - t_2)^{-1}$  is the rate window, proportional to the emission rate of the defects. In the case of wide-bandgap semiconductors, the capacitive transients associated with electron emission do not necessarily have the ideal exponential trend reported in equation (6). This can be related to the mixed exponential transients due to the emission from several defects, non-exponential transients associated with complex energy, or space distribution of deep levels or others. Therefore, it is usually more convenient to directly analyze the capacitance transient associated with the carrier emission, and then extract the time constants by performing a multiple pure or stretched exponential fitting.

The amplitude of the capacitance transient  $\Delta C$  is associated with the concentration of deep levels, according to [29, 77]

$$\frac{N_T}{n} = 1 - \left(1 - \frac{\Delta C}{C_\infty}\right)^2 \approx 2 \frac{\Delta C}{C_\infty} \quad (8)$$

where  $C_\infty = C(t \rightarrow \infty)$  and the first equality have a general validity, while the approximation holds for a small capacitive transient ( $\Delta C/C_\infty < 1$ ).

Among other measurement parameters, the filling time  $t_f$  has pivotal importance in the C-DLTS analysis, since it is strictly connected to the number of trapped carriers in the semiconductor; its impact on the measurements can provide information on the dimensionality of the defects, as well

as their energy distribution, by analyzing the carrier capture kinetics [68, 69].

In the case of non-interacting point defects, the capture process consists of the relaxation of the electrons (or holes) from the conduction (or valence) band. This process has a constant capture rate  $c_n = v_{th} \sigma_n$ , which results in a C-DLTS signal that exponentially depends on the filling pulse width  $t_f$  [78]:

$$S(t_f) = S_\infty (1 - e^{-c_n t_f}). \quad (9)$$

As previously discussed, during the thermal capture the electron has to overcome the capture barrier  $\Phi_B$  by gaining sufficient thermal energy (figure 4(a)). In the literature, this process was correlated with an exponential dependence of the apparent capture cross-section  $\sigma$  with the temperature [69, 70]:

$$\sigma(T) = \sigma_\infty e^{-\frac{q\Phi_B}{k_B T}}. \quad (10)$$

The presence of a capture barrier introduces an additional term to the activation energy detected by C-DLTS. According to figure 4(a), the trapped electrons must obtain an energy greater than  $\Delta E = E_{A,th} + q\Phi_B$  to be promoted to the conduction band, and equation (5) becomes

$$e_n = \frac{\sigma_n v_{th} N_C}{g} \exp\left(-\frac{q(E_{A,th} + \Phi_B)}{k_B T}\right). \quad (11)$$

If defects are clustered, for example, along a dislocation, the related states can interact due to the time-dependent coulombic potential  $\Phi(t)$  generated by the trapped electrons. In this case, the trapping rate is described by the following equation [79]:

$$\frac{dn_T(t)}{dt} = c_n (N_T - n_T(t)) e^{-\frac{q\Phi(t)}{kT}}. \quad (12)$$

The coulombic potential is proportional to the concentration of trapped defects  $n_T$ , and can be represented as follows [79]:

$$\Phi(t) = \Phi_0 \frac{n_T(t)}{n_{T,0}} \quad (13)$$

where  $n_{T,0}$  is the number of trapped states for  $t=0$ . Equation (12) has a logarithmic solution under the hypothesis that  $n_T(t) \ll N_T$  [79, 80]:

$$\frac{n_T(t_f)}{N_T} = c_n \tau n \log\left(\frac{t_f + \tau}{\tau}\right), \quad (14)$$

in which the time constant  $\tau$  is a fitting parameter.

In the case where the deep levels are distributed in energy, the classical exponential emission equation (equation (6)) is no longer valid, because each sub-level is characterized by its own time constant according to equation (5). Empirically, this leads to a stretched exponential emission transient according to [81]:

$$n_T(t) = N_T \left[ 1 - \exp\left(-\left(\frac{t}{\tau_n}\right)^\beta\right) \right], \quad (15)$$

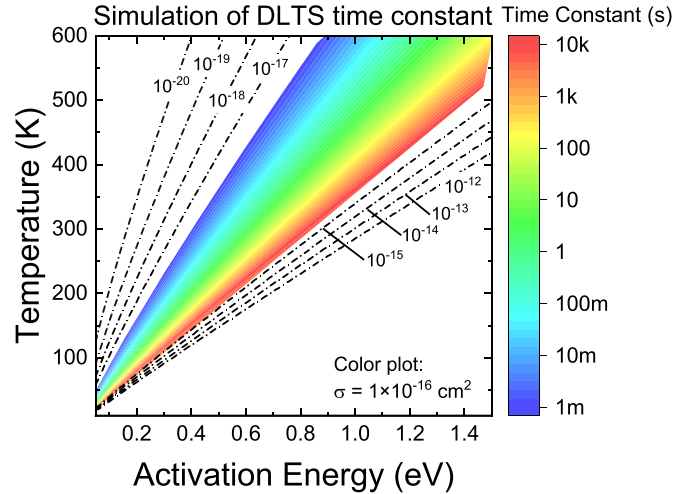


**Figure 6.** Calculation of the emission time constants from a deep level as a function of the activation energy and temperature. From a practical point of view, only defects with  $E_A < 1.5$  eV can be detected by DLTS, thus requiring other measurement techniques for deeper levels.

in which  $\beta$  is the exponential stretching factor. The presence of a deep-level energy band can also be detected by analyzing the DLTS peak as a function of the filling time. In fact, since the trapped electrons thermalize to lower energy levels, first the deeper states are filled, resulting in higher detected activation energies for shorter filling pulses. Considering the C-DLTS signal defined in equation (7), this causes a shift toward lower temperatures at higher filling pulses [82], while the temperature of the peak is independent of the temperature for non-interacting point defects [83].

Since the characteristic emission time constant from a deep level depends exponentially on the activation energy and temperature, it follows from equation (5) that deep levels featuring a high activation energy can be probed in a reasonable amount of time only at high temperatures. The instrument limitations (typically 1 ms to 10 ks) and the maximum storage/operating temperature of the devices ( $20 \text{ K} < T < 600 \text{ K}$ ) pose the boundaries of the detection limits of C-DLTS experiments.

In figure 6 the emission time of a deep level with a capture cross-section  $\sigma = 1 \times 10^{-16} \text{ cm}^2$  is calculated according to equation (5) as function of the activation energy and absolute temperature. It is clear that DLTS finds application for deep levels approximately between 0.1 eV to 1.5 eV, a range that is too limited for a full bandgap characterization of a wide-bandgap semiconductor, which can be higher than 4 eV.

Starting from the work of Lang [29], the basic C-DLTS technique was further developed by many authors. In general, the analysis technique used for these measurements recalls the basic approach discussed in the previous paragraph, following which a trapping-dependent device property is measured over time as a function of external stimuli to infer on specific trap properties: for this reason it will not be discussed in great detail.

Current DLTS, also called I-DLTS, is a technique that exploits current transients rather than the capacitance

transients [84, 85], and is capable of providing an excellent sensitivity (up to  $N_T/n \approx 10^{-8}$ ). This technique is often exploited for the characterization of transistors, whose drain current can be easily monitored after applying a proper gate or drain stress.

Double-correlation DLTS (DDLTS) was proposed by Lefevre and Schulz [86], and consists of a variation of the standard C-DLTS procedure, which considers the difference in capacitance between two emission capacitance transients induced by two (slightly) different filling pulses ( $V_{f,1} < V_{f,2}$ ). This method is usually preferred over the standard C-DLTS because it enables us to probe a narrower volume within the SCR, thus eliminating the estimation errors due to the field dependence of the emission coefficient and due to the partial trap filling in the Debye tail [87].

Constant-capacitance DLTS (CC-DLTS) [88–90] exploits a feedback loop to keep the device capacitance constant during the measurement interval by continuously changing the applied voltage. In this way, the SCR width is always constant during the measurement, thus allowing a more accurate estimation of the deep-level profiles, especially in the presence of high defect densities. Moreover, this approach can also be adopted to characterize deep levels located at the interface of metal-oxide-semiconductor (MOS)-like structures [91–93]. Eventually, this technique can be combined with the DDLTS to get the benefit from both techniques [94].

Alternatively, by means of the so-called optical DLTS (O-DLTS), traps can be filled or emptied by a sub-bandgap light pulse that replaces the conventional voltage filling pulse [95, 96]. The use of light enables easy detection of minority carrier traps in unipolar devices, and an understanding of some of the optical properties of deep levels.

#### 4.2. DLOS

As previously mentioned, the detection range of DLTS-like measurements is limited by the characteristic time constants of the defects, and therefore by the experimental time and temperature constraints. To overcome these limitations, especially for deep levels located more than 1 eV (see figure 6) from the respective band edge, it is more convenient to consider the response of the deep levels to optical stimulation.

DLOS is an experimental technique that allows the characterization of the optical properties of deep levels by monitoring the capacitance transients associated with the light-stimulated emission of the trapped carriers [31]. The main advantage of this technique is the wide detection range, which goes from a few hundredths of eV (by exposing the samples to infrared light) to several eV (ultraviolet), thus enabling the full bandgap of most of wide-bandgap semiconductors to be probed.

In principle, DLTS and DLOS are complementary techniques, not only for different detection ranges, but also for the different physical properties considered for the measurement.

The effect of light excitation on semiconductors was originally analyzed by Furukawa [97], who observed a change in the junction capacitance during light illumination at cryogenic temperatures in GaAs SBDs due to charge detrapping from deep levels. In general, light excitation can induce two

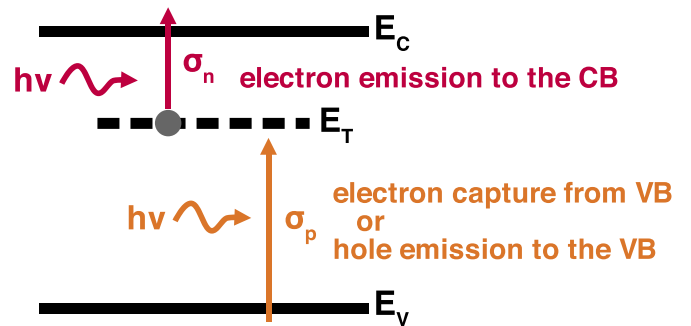


**Figure 7.** Schematic representation of the optical transitions involved in DLOS measurement. In case of an acceptor-like defect, light can stimulate the emission of a trapped electron to the conduction band, or the capture of an electron from the valence band to an empty trap state.

competing processes, schematically represented in figure 7: first, the photons can excite the electrons from the trap state to the conduction band (optical excitation, described in section 3.1); second, photons can promote the electrons from the valence band to the trap state, resulting in light-induced trapping (not shown in the GCCD).

It follows that the trap occupation is described by the following rate equation [98]:

$$\frac{dn_t}{dt} = -\sigma_n^O(h\nu) \Phi(h\nu) n_t + \sigma_p^O(h\nu) \Phi(h\nu) p_t, \quad (16)$$

in which  $\Phi$  [ $\text{cm}^{-2} \text{s}^{-1}$ ] is the photon flux at a given energy,  $\sigma_n^O$  [ $\text{cm}^2$ ] is the optical cross-section of the electron emission process, and  $\sigma_p^O$  [ $\text{cm}^2$ ] is that of electron capture (hole emission to the valence band). From the spectral dependence of  $\sigma_n^O$  and  $\sigma_p^O$ , based on appropriate models [99, 100], one can obtain a full description of the trap parameters in terms of the optical activation energy  $E_O$  and the Frank–Condon shift  $d_{FC}$ .

The values of  $\sigma_n^O$  and  $\sigma_p^O$  assume different values depending on the trap occupation before the experiment, which can be appropriately selected with different filling conditions. Let us consider as an example an n-type SBD: if the filling phase consists of a forward pulse, the majority carriers are trapped in the deep levels, resulting in  $\sigma_n^O \gg \sigma_p^O$  [31]. In this case, the contribution of  $\sigma_p^O$  can be neglected, and equation (16) simplifies as

$$\frac{dn_t}{dt} = -\sigma_n^O(h\nu) \Phi(h\nu) n_t(h\nu). \quad (17)$$

On the other hand, when considering bipolar devices such as  $p-n$  junctions, a forward-bias filling pulse results in the injection of minority carriers along with the majority ones, and this leads to a possible intermix of the effects of both types of carriers.

Under the hypothesis that the deep levels are totally filled before light exposure ( $n_T(t=0) = N_T$ ),  $\sigma_n^O(h\nu)$  can be extracted as:

$$\sigma_n^O(h\nu) = -\frac{1}{\Phi(h\nu) N_T} \times \left( \frac{dn_t}{dt} \right)_{t=0}. \quad (18)$$

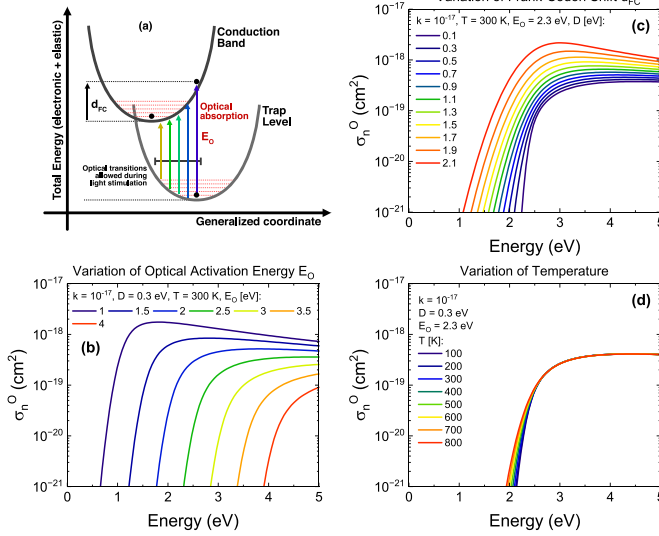


**Figure 8.** (a) Origin of the optical broadening of the PCS: the electrons can occupy different vibrational levels in the trap state, and therefore many different optical transitions are allowed. Variation of the PCS according to the Pässler model as a function of (b) optical activation energy, (c) Frank–Codon shift, and (d) temperature.

By integrating equation (17) and supposing a constant photon flux and optical cross-section over time, the optical emission transient can be described by the exponential function  $n_T(h\nu, t) = N_T(h\nu) \exp(-t/\tau(h\nu))$ , and therefore the optical cross-section can be easily obtained as:

$$\sigma_n^O(h\nu) = \frac{1}{\Phi(h\nu)\tau(h\nu)}. \quad (19)$$

As discussed in section 3, the presence of a non-zero Frank–Codon shift results in a misalignment between the parabolas associated with the trapped and excited states. Since the electrons assume different vibrational energy levels, the optical response is broadened according to the statistical occupation of the electrons in the trap sub-states (figure 8). In the case of a pure optical transition between the trapped and the excited state ( $d_{FC} \rightarrow 0$ ),  $\sigma_n^O(h\nu)$  is independent of the temperature and can be described through the semiclassical model proposed by Lukowsky in 1965 [100]. The thermal binding energy  $E_A$  can be extracted in a rather simple form as

$$\sigma^O(h\nu) \propto \frac{E_{A,O}^{1/2}(h\nu - E_{A,O})^{3/2}}{(h\nu)^3} \quad (20)$$

In the case of stronger electron–lattice coupling, the MPE or absorption process needs to be taken into account; this is usually done by solving a convolution integral supposing that the electrons have a linear interaction with the harmonic lattice oscillations. By assuming a Gaussian dependence of the thermal broadening of the photoionization cross-section (PCS), Pässler [99] estimated  $\sigma_n^O(h\nu)$  as:

$$\begin{aligned} \sigma^O(h\nu, T) \cong & \frac{K}{h\nu \sqrt{2\pi d_{FC}\varepsilon \coth\left(\frac{\varepsilon}{2k_B T}\right)}} \\ & \times \int_0^\infty \frac{E_K^{\frac{3}{2}}}{(E_K + E_O - d_{FC})^2} \\ & \times \exp\left[-\frac{h\nu - E_O - E_K}{2d_{FC}\varepsilon \coth\left(\frac{\varepsilon}{2k_B T}\right)}\right] dE_K \end{aligned} \quad (21)$$

where  $\varepsilon = \hbar\bar{\omega}$  is the effective phonon energy,  $E_K = E_e - E_T$  is the kinetic energy of the excited electron, and the other constants have the usual meaning. In figure 8, the Pässler model for the PCS is reported as a function of different (b) optical activation energies  $E_O$ , (c) Frank–Codon shifts  $d_{FC}$ , and (d) temperature. It is worth noting that low Frank–Codon shifts ( $d_{FC} \ll E_O$ ) result in a sharp PCS, while high  $d_{FC}$  values are associated with a higher dispersion of the PCS; this is due to the fact that a higher  $d_{FC}$  results in less overlap between the parabolas of the trapped and excited states in the GCCD, and therefore more vibrational sub-levels can be involved in an optical transition.

The experimental procedure for DLOS is schematically reported in figure 9. The first step consists of a fill phase, in which the junction is forward biased for a certain time  $t_{fill}$  in order to fill the levels in the space charge. Second, the junction is biased at the measurement voltage  $V_m$  to favor the thermal emission of relatively shallow deep levels in a C-DLTS-like transient. Finally, once the thermal transient is settled, monochromatic light is shone onto the sample, and the optically-induced transient is sampled until reaching steady state. The steady-state photocapacitance (SSPC, i.e. the capacitance of the junction after the settling of the light-induced transient) provides information on the defect concentration as a function of the photon energy [10, 31]:

$$\frac{N_T(h\nu)}{N_D} \cong 2 \frac{\sigma_n^O(h\nu) + \sigma_p^O(h\nu)}{\sigma_n^O(h\nu)} \frac{\Delta C(h\nu)}{C_0} \approx 2 \frac{\Delta C(h\nu)}{C_0}, \quad (22)$$

where  $C_0 = C(t_{light} = 0)$  and  $\Delta C(h\nu) = C(t_{light} \rightarrow \infty) - C_0$  and the second approximation holds in the case where the optical filling process is negligible with respect to the optical emission ( $\sigma_n^O \gg \sigma_p^O$ ).

With the same hypothesis, and by combining equations (18) and (22), the PCS can be extracted from the capacitance transients as

$$\sigma_n^O(h\nu) = -\frac{1}{\Phi(h\nu)\Delta C} \times \left( \frac{dC}{dt} \right)_{t=0}. \quad (23)$$

It is worth highlighting that DLOS and O-DLTS have some intrinsic differences that can lead to misinterpretation of the experimental results. The main difference between the two techniques is that O-DLTS monitors the capacitance transient *after* the light exposure, thus leading to a thermal capacitance

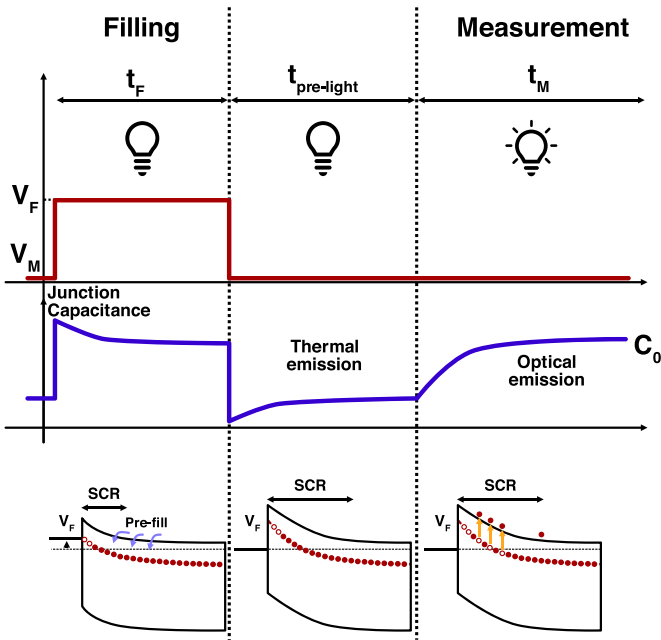


**Figure 9.** Typical measurement sequence for the deep-level optical spectroscopy technique. The measurement consists of three phases: (i) first, the deep levels in the SCR are pre-filled with a forward pulse; (ii) then, the junction is kept in dark conditions to favor the emission from shallow deep levels; (iii) finally, monochromatic light is applied to the junction, thus inducing the optical emission of trapped carriers.

transient, whereas for DLOS we have an optically-stimulated transient recorded during light-induced carrier de-trapping. Considering this, the outcome of the two methods is also different: time constants associated with O-DLTS measurements can provide information on the thermal emission rate of specific traps, and therefore on their thermal activation energy and capture cross-section, whereas DLOS-related transients can be computed to derive the PCS of the responding trap.

#### 4.3. Characterization of deep levels in transistors

The detection of deep-level defects in more complex structures such as transistors is not straightforward, because the device may contain several layers made of different materials, and the doping concentration and the defects can be localized in a number of device regions and contribute to effects associated with parametric instability. Usually, trap detection is based on a set of experiments that conceptually follow the DLTS measurement scheme. The traps are usually filled during a stress phase, and then the carrier emission is monitored during the recovery phase. During the experiment, the evolution of device parameters such as the threshold voltage, gate capacitance, ON-resistance, and others is monitored as a function of the stress (or recovery) time and applied bias. For instance, the evolution of the threshold voltage or the gate capacitance is usually correlated with traps in the gate insulation in MOSFETs [101–103], or the AlGaN barrier in HEMTs [104, 105], which is sometimes also coupled with inhibition effects due to defects clustered close to the transistors' channel

[106, 107]. Moreover, the analysis of the dynamic  $R_{ON}$  or the drain current during stress can provide information on defects in the buffer layer [6, 7, 108] or in the passivation [109, 110]. The results are usually analyzed following the DLTS procedure: the experimental data are usually fitted with exponential or stretched exponential relations to obtain the characteristic time constants, from which the Arrhenius plots and activation energies can be obtained.

#### 5. Case study: analysis of deep levels in N-doped $\beta$ -Ga<sub>2</sub>O<sub>3</sub>

In this section, we will discuss a case study on the detection of deep defects in nitrogen-implanted  $\beta$ -Ga<sub>2</sub>O<sub>3</sub> SBDs, whose schematic cross section is reported in figure 10. The samples under test consist of an unintentionally doped ( $n \approx 2 \times 10^{17} \text{ cm}^{-3}$ )  $\beta$ -Ga<sub>2</sub>O<sub>3</sub> edge defined film-fed grown (EFG) bulk crystal, in which nitrogen ions were implanted with an energy of 480 keV and a dose of  $4 \times 10^{13} \text{ cm}^{-2}$ . The back-side ohmic contact was formed by implanting Si with a target concentration  $n^+ = 5 \times 10^{19} \text{ cm}^{-3}$ , activated by rapid thermal annealing (RTA) at 800 °C for 30 min in N<sub>2</sub> atmosphere. The implantation damage was partially recovered with an RTA treatment at 900 °C (for 30 min in N<sub>2</sub>). Additional information on the samples under test can be found in [111].

In previous works that considered the same samples reported here, we demonstrated that the samples are affected by a turn-on voltage instability due to the presence of intrinsic deep levels possibly related to the displacement damage induced by the nitrogen implantation, and whose concentration decreases at increasing annealing temperatures [1, 2]. Recently, Ghadi *et al* carried out an extensive study on the deep-level defects induced by nitrogen implantation and found that N impurities are possibly related to a deep level with  $E_O = 4.3 \text{ eV}$  and a  $d_{FC} = 1.4 \text{ eV}$  [112].

For the DLOS experiment, devices were filled with a forward pulse of 3 V for 60 s, and then biased at 0 V in dark conditions for 600 s to allow thermal emission from the shallower levels. Finally, monochromatic light obtained with a Xe arc lamp and a monochromator was shone on the samples. The measurement time under the light was appropriately selected to ensure that the transients were settled, or eventually to not exceed a transient time of 1000 s. The typical capacitance transients for the pre-light, light, and post-light conditions are reported in figure 11.

The analysis of the SSPC and the PCS was performed by considering the light transients reported in figure 12. By looking at the shape of the curves, we note three different behaviors: first, for low photon energies ( $E_{ph} < 3.2 \text{ eV}$ ), we have a single exponential transient with a time constant that progressively decreases with energy, as expected from the Pässler model for a single deep level (hereafter labeled E6, following the trap nomenclature used in section 6). Then, at intermediate photon energies ( $3.2 \text{ eV} < E_{ph} < 3.7 \text{ eV}$ ), we notice the onset of another exponential component associated with the presence of a second electron trap labeled E<sub>N</sub>, which again exhibits time constants strongly activated by the photon energy. It

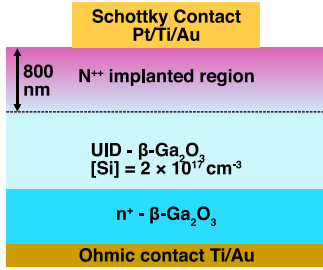


**Figure 10.** Schematic cross-section of the devices under test [25].

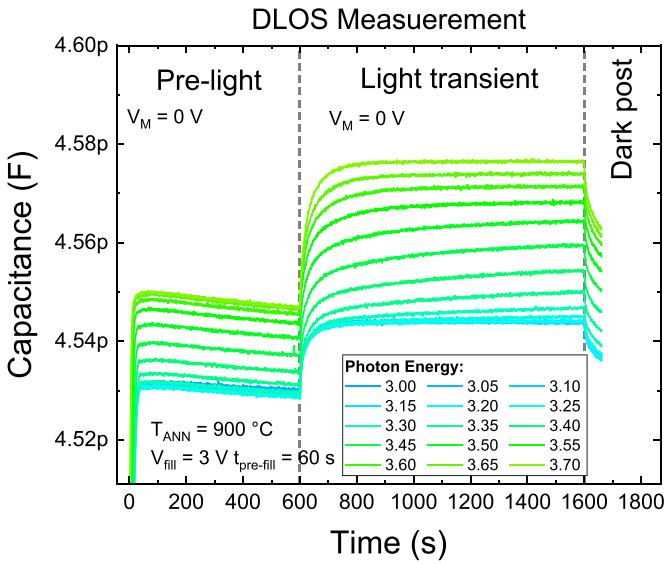


**Figure 11.** Capacitance transients associated with the DLOS experimental procedure during (i) pre-light, (ii) light transient, and (iii) dark post-light for a selected number of photon energies.

is worth noting that the time constants associated with E6 are approximately constant at high photon energies: this is due to the particular shape of the PCS spectrum, which usually saturates for energies approximately above the optical activation energy. The transients were fitted with two exponential terms, appropriately selected to model the contribution of the two traps E6 and  $E_N$ . At this point, the SSPC can be defined for each defect as the normalized exponential transient amplitude with respect to the dark (pre-light) capacitance value  $C_0$ . The results indicate that the SSPC associated with the trap E6 monotonically increases in the range 1.5 eV–3.0 eV, and reaches a maximum normalized concentration of  $N_T(E_x)/n \cong 4 \times 10^{-3}$ , whereas the transients associated with the trap  $E_N$  reach a maximum amplitude at around 4.2 eV and  $N_T(E_Y)/n \cong 2 \times 10^{-2}$ . The defect concentration of the trap  $E_N$  is in the same range as that of the trap E2 and E3 already detected by DLTS in our previous work [1], while trap E<sub>x</sub> has a much lower density.

For the analysis of the PCS, we will present two alternative approaches. Traditionally, the PCS is extracted according to equation (23), i.e. by considering the derivative of the light transient for  $t = 0$ . If we consider a generic DLOS capacitive

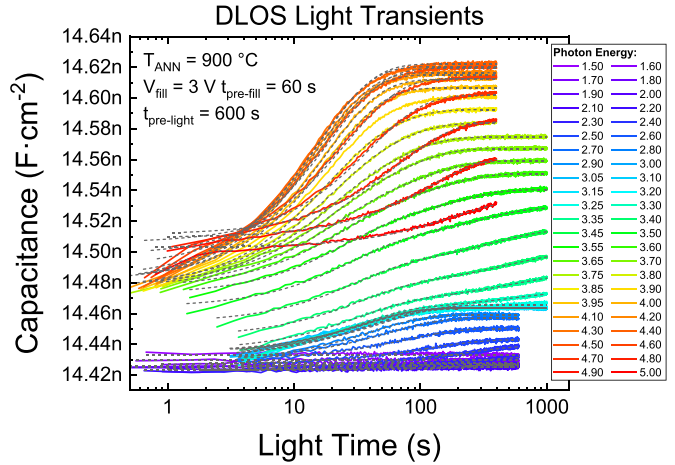


**Figure 12.** DLOS light transients at different photon energies. For low photon energies ( $E_{ph} < 3.2\text{ eV}$ ), the transients have a single exponential component due to the presence of trap E6, and at higher photon energies we have the onset of the second exponential component due to the presence of  $E_N$ .

transient for a semiconductor with multiple deep levels, this can be expressed in the form

$$C(t, h\nu) = C_0 + \sum \Delta C_i(h\nu) \exp\left(-\frac{t}{\tau(h\nu)}\right), \quad (24)$$

in which  $\Delta C_i$  is the amplitude of each exponential component as a function of the incident photon energy. According to equation (23), the PCS can be obtained as

$$\sigma_n^O(h\nu) \cong \frac{1}{\Phi(h\nu) \Delta C(h\nu)} \times \sum \frac{\Delta C_i(h\nu)}{\tau(h\nu)}. \quad (25)$$

Owing to the presence of the sum of several different contributions, the term  $\Delta C$  has to be properly selected to factor out the  $\Delta C_i$  terms for each defect. By considering the Pässler model for the PCS (see (c)), and by assuming that the deep levels are well separated from one another, i.e. at each photon energy only one deep level dominates the exponential transient, a condition empirically obtained if  $E_i + d_{FC,i} < E_{i+1} - d_{FC,i+1}$ ,  $\Delta C$  can be defined as

$$\overline{\Delta C(h\nu)} = \max_i \{\Delta C_i(h\nu)\}. \quad (26)$$

The PCS obtained with the approach presented above is plotted in figure 14. The label ‘Total PCS’ was adopted in order to underline that the signal is obtained by the contribution of the PCS of the two different deep levels. This approach provides a reasonable estimation of the PCS whenever the defects are separated in terms of the optical activation energy but creates a non-negligible error in the energy range in which both defects are responding. In addition, the extraction of the derivative of the light transient for  $t = 0$  is not straightforward, because it requires a fast sampling of the capacitance that is not usually easy to obtain with commercially available instruments.

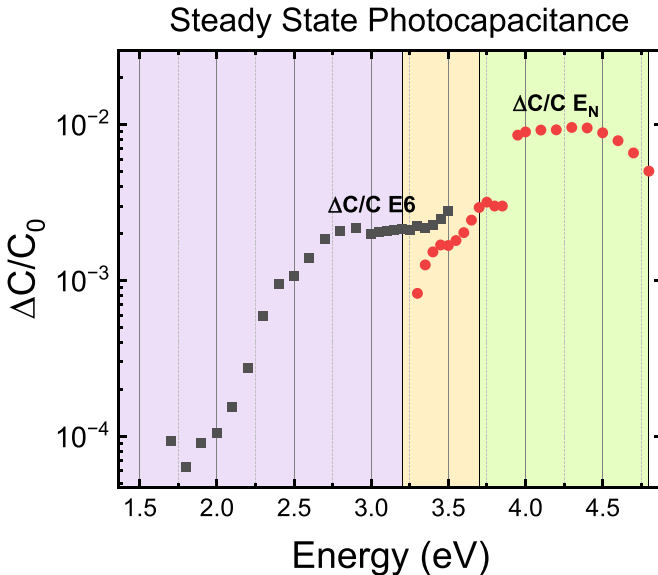


**Figure 13.** SSPC extracted with a double exponential fitting of the experimental data.

Alternatively, the PCS can be obtained by applying equation (19) separately for each time constant obtained from the multi-exponential fitting of the light transients. In this way, we can obtain a separate PCS signal for each defect, which can be fitted with an appropriate model. This new approach has the advantage of being more selective with respect to the optical response of different defects but requires an adequate sampling of the capacitance transient (a large number of samples at the beginning of the light transient and a careful exponential fitting). The improvements with respect to the traditional analysis can be appreciated, especially in the energy range between 3.2 eV and 3.4 eV, where the sampled capacitance transient is strongly influenced by both defects. To conclude the analysis, trap parameters were extracted by fitting the PCS data with the Pässler model, as reported in equation (21) [99]. Trap E<sub>6</sub> presents an optical activation energy  $E_O = 2.59$  eV and a  $d_{FC} = 1.21$  eV, whereas the trap E<sub>N</sub> has  $E_O = 3.66$  eV and a  $d_{FC} = 0.32$  eV. It is worth noting that owing to the separation between the two exponential contributions, the estimation of the parameters of trap E<sub>N</sub> can be obtained by fitting the PCS in two orders of magnitude of amplitude. By looking at figure 14 in the lowest energy range ( $2.0 < E_{ph} < 2.25$  eV), one may notice an apparent decrease of the PCS data at higher photon energies. This phenomenon can be attributed to an error in the estimation of the time constants due to the low transient amplitude (figure 13). On the other hand, the decrease of the PCS in the high-energy range ( $E_{ph} > 4.55$  eV) is associated with the partial absorption of the photons by the semiconductor layers ( $E_g \sim 4.85$  eV) and subsequent  $e-h$  pair generation.

## 6. Review of deep levels in $\beta\text{-Ga}_2\text{O}_3$

Research on the deep-level defects in  $\beta\text{-Ga}_2\text{O}_3$  bulk crystals and epitaxial layers has been particularly active in recent years,

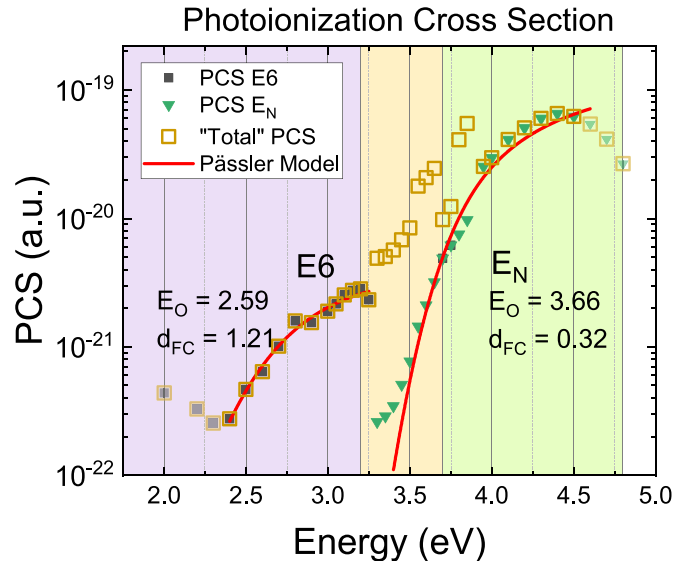


**Figure 14.** PCS of the two electron traps identified by DLOS, obtained through traditional approach based on the calculation of the derivative of the capacitive transient, and with the novel approach that extract the spectral dependence based on the separate analysis of each time constant.

with several literature contributions to the detection based on C-DLTS, DLOS, TAS, and others. When considering the deep levels in  $\beta\text{-Ga}_2\text{O}_3$ , it is common practice to use the nomenclature originally proposed by Irmscher *et al* [113] and further extended by Wang *et al* [77]. In figure 15 the Arrhenius plots of the trap signatures detected in several literature reports are shown.

Trap E1 ( $E_C = 0.60$  eV) is found in several  $\beta\text{-Ga}_2\text{O}_3$  references [113–118]. The concentration of the deep level has a weak dependence on the irradiation process. The origin of this trap is still ambiguous, but some authors suggest a possible involvement of transition metal impurities [116].

Trap E2 ( $E_C = 0.80$  eV) is one of the most common defects in  $\beta\text{-Ga}_2\text{O}_3$ , and is commonly found in both bulk materials and epitaxial layers [1, 68, 113, 115, 119–123], and commonly associated with substitutional Fe impurities (Fe<sub>Ga</sub>) [77, 114] that may be introduced in crystals during the bulk growth of Czochralski and EFG substrates [124, 125] or intentionally introduced in the devices to compensate residual donors. Recently, Zimmerman *et al* demonstrated that the level E2 is composed of two sub-levels, E2a and E2b, respectively related to the Fe<sub>Ga</sub> substitutional impurities in the tetrahedral (Fe<sub>Ga(I)</sub>) or octahedral (Fe<sub>Ga(II)</sub>) sites [126]. The possible role of Fe in trap E2 was also demonstrated by McGlone *et al*, and demonstrates that the introduction of a thick UID buffer layer can suppress the formation of the trap responsible for the threshold voltage instability in lateral metal-semiconductor field effect transistors (MESFETs) [119, 127].

However, the impact of high-energy irradiation and implantation is still unclear: [114, 128, 129] suggest that the concentration of E2 is not strongly affected by high-energy proton irradiation, while a study by Polyakov *et al* [116] shows an increase in concentration of roughly one order of magnitude.

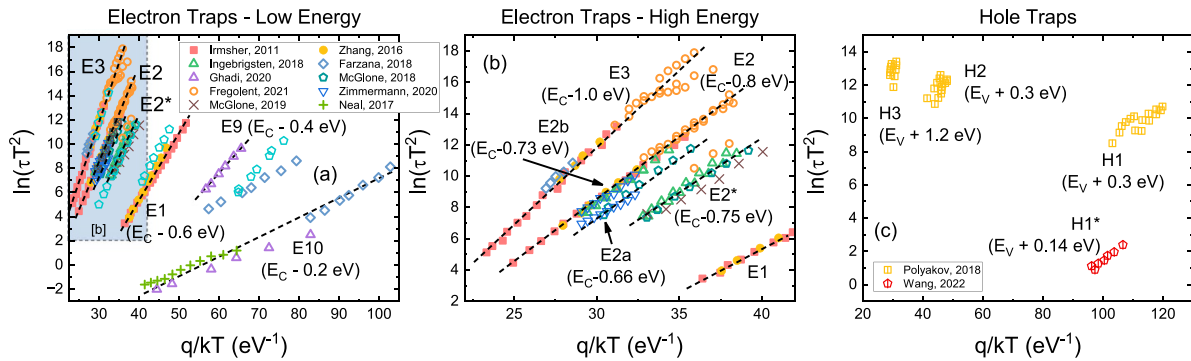


**Figure 15.** Arrhenius plot of the most common deep levels in  $\beta\text{-Ga}_2\text{O}_3$  detected by DLTS-like experiments. (a) Low and high activation energy traps, (b) high activation energy traps, (c) minority carrier traps.

Trap E2 was also found to be responsible for charge trapping in nitrogen-implanted SBDs [1, 2], with a concentration that decreases at high annealing temperatures. Considering the latter results and the fact that the trap is commonly found in high-quality epi-layers, we previously proposed that the trap E2 may also not be strictly correlated with the iron impurities, but related to a native point defect whose concentration is possibly enhanced by the presence of Fe [1], a behavior already detected in Fe-doped GaN [108].

Trap E2\* ( $E_C$ -0.75 eV) is associated with an intrinsic defect possibly related to  $V_{\text{Ga}}$  or  $\text{Ga}_0$ , since its concentration is strongly enhanced with radiation damage [116, 117, 128–130]. This level was also found by McGlone *et al* [119, 127] in MESFETs grown by plasma assisted molecular beam epitaxy (PAMBE), and by Fregolent *et al* in N-implanted samples annealed at 1200 °C [1]. The formation and passivation of this level was deeply discussed in [120], where the divacancy ( $V_{\text{Ga}}-V_{\text{O}}$ ) was proposed as a possible candidate for the defect.

Trap E3 ( $E_C$ -1.0 eV) is another common level found in both bulk crystals and epitaxial layers [1, 113, 115, 116, 126, 130]. The interpretation of the origin of this level has always been unclear, but recently Zimmerman *et al* proposed a possible involvement of the substitutional defect  $\text{Ti}_{\text{GaII}}$  [126]. This result is particularly important since many metallization schemes use Ti as a metal, and this can be a source of contamination.

Trap E4 ( $E_C$ -1.2 eV) has higher activation energy and is commonly detected by DLOS either on epitaxial layers or bulk crystals [117, 118, 130, 131]; its density was shown to increase with high-energy proton irradiation [132], and therefore the level is likely to be associated with a native point defect.

Trap E6 ( $E_C$ -2 eV) has been extensively investigated by means of DLOS by several authors [115, 122, 130, 132] because its formation is related to high energy, and it is correlated with the compensation and carrier removal induced by the radiation damage [131]. These findings suggest that the traps are possibly related to vacancies, or complex defects involving vacancies and self-interstitials, such as  $2V_{\text{Ga}}-\text{Ga}_i$  [131].

Trap E8 ( $E_C$ -4.4 eV) is another common trap of  $\beta\text{-Ga}_2\text{O}_3$  regardless of the growth method [115, 122, 130–132], and it is usually characterized by a small  $d_{FC} \approx 0.05$  eV. Originally, the trap was believed to be due to the presence of self-trapped holes with activation energy close to the valence band edge,

and already predicted by theoretical calculation [133]. This level was also detected as a minority (hole) trap located at  $E_V + 0.22$  eV by Polyakov *et al* by means of O-DLTS (H1 in figure 15(c)) [134] and by Wang *et al* [135] ( $E_V + 0.20$  eV, H1\* in figure 15(c)). However, this interpretation is in contradiction with the fact that the concentration of the level is much lower in metalorganic chemical vapor deposition (MOCVD)-grown material [131], and presents a little dependence with proton fluence during irradiation [118, 132]; therefore, it is currently believed that it originates from extrinsic causes.

Trap E9 ( $E_C$ -0.40 eV) was detected by Ghadi *et al* [131] on an MOCVD-grown epi-layer, and it is associated with an intrinsic point defect.

Trap E10 ( $E_C$ -0.20 eV) is a shallow donor trap found in a variety of different material types, including bulk crystals [136], and epitaxial layers grown by MOCVD [131], PAMBE [130], and halide vapor phase epitaxy (HVPE) [117]. This level was attributed to the substitutional level  $\text{Si}_{\text{GaII}}$ , which originates from silicon contamination or doping [136].

Trap  $E_N$  ( $E_C$ -3.1 eV) was mentioned by Ghadi *et al* [112] and by this work, and it is associated with deep nitrogen acceptors, possibly related to  $\text{N}_{\text{O(III)}}$ .

In addition to the aforementioned trap H1, some other works have reported other minority carrier traps in  $\beta\text{-Ga}_2\text{O}_3$  [117, 134]. In [134], Polyakov *et al* found two trap signatures labeled H2 ( $E_V \pm 0.0.3\text{--}0.4$  eV), possibly related to an electron capture barrier, and H3 ( $E_V \pm 1.3\text{--}1.4$  eV), tentatively associated with gallium vacancies [116, 117, 134].

The position of the deep levels with respect to the conduction and valence band edges is summarized in figure 16.

As can be noted from the references cited in the previous paragraphs, many works on the detection of deep levels in  $\beta\text{-Ga}_2\text{O}_3$  are focused on the analysis of high-energy particle irradiation [137], including neutrons and protons. This is motivated by the fact that  $\beta\text{-Ga}_2\text{O}_3$  is generally considered a radiation-hard material, and the analysis of the deep-level formation in harsh environments is therefore of pivotal importance.

To date, there have been no literature reports specifically dealing with the formation of deep levels as an effect of other driving stress forces, such as high temperature or strong electric fields.

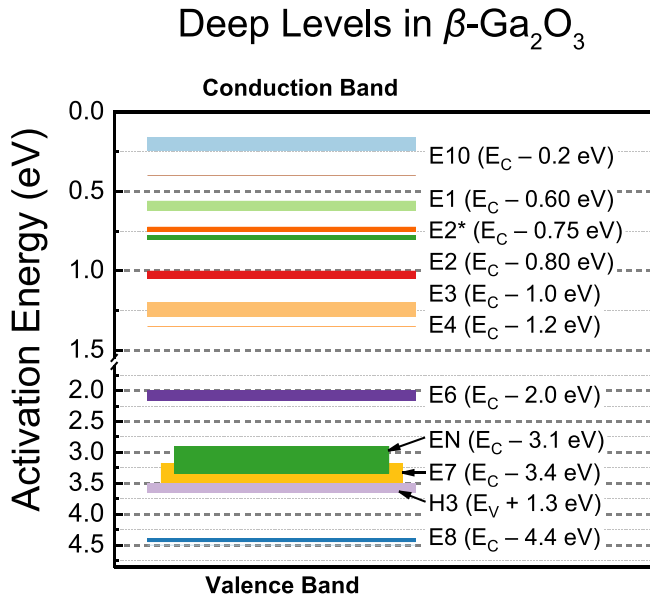


**Figure 16.** Energy distribution of the common deep levels in  $\beta\text{-Ga}_2\text{O}_3$  with respect to the conduction and valence band edges.

## 7. Review of deep levels in GaN

Despite the maturity of the crystal growth and device processing, deep levels in GaN are still responsible for many device non-idealities. In general, the growth of GaN is still prone to the formation of native defects involving vacancies, interstitials, and antisites of both nitrogen and gallium atoms ( $V_N$ ,  $N_I$ ,  $N_{Ga}$ ,  $V_{Ga}$ ,  $Ga_I$ ,  $Ga_N$ ). An overview of the most common intrinsic defects of GaN is reported in figure 17(a).

Nitrogen interstitials ( $N_I$ ) are responsible for the formation of deep levels located approximately at  $E_C - 0.9$  eV [138–141]. Owing the rather high activation energy, these levels are between the most effective trapping and G-R centers, leading to strong SRH recombination.

Nitrogen vacancies ( $V_N$ ) are among the most common intrinsic traps of GaN, typically found close to the  $E_C - 0.24$  eV level. In the literature, this deep level is associated with both point and extended defects [142–149], or eventually related to complexes such as vacancy clusters [150, 151]. In addition,  $V_N$  have been proposed as sources of green and red luminescence [152, 153] in bulk materials and in quantum wells [154].

Nitrogen antisites ( $N_{Ga}$ ) are associated with the formation of point defects located between  $E_C - 0.65$  eV and  $E_C - 0.50$  eV [139, 142, 143, 148, 155, 156].

Gallium interstitials ( $Ga_I$ ) were reported by two references [141, 157], in which it is and are considered to form a deep level at  $E_C - 0.8$  eV (associated with dislocations) and  $E_C - 0.91$  eV.

Gallium vacancies ( $V_{Ga}$ ) are commonly associated with a deep level located at  $E_C - 2.6$  eV [140, 141, 148, 158, 159]. It is reported that  $V_{Ga}$  has the tendency to interact with other defects and form a complex with oxygen [141, 160],

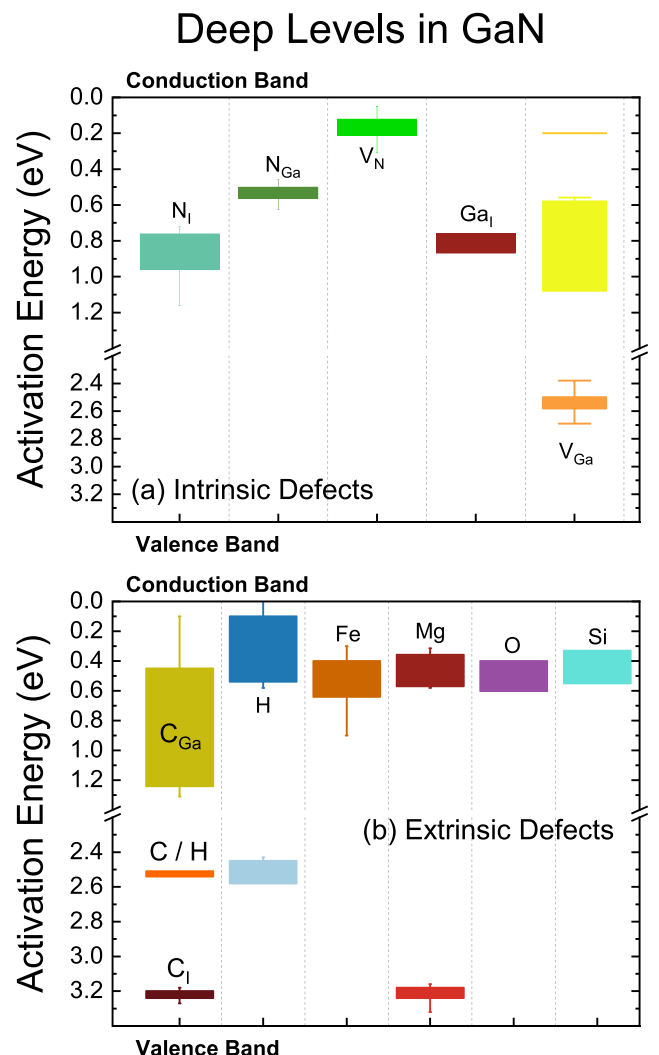


**Figure 17.** Overview of the position of common (a) intrinsic and (b) extrinsic deep levels in gallium nitride. The energy position of the deep levels was obtained by a wide literature review that considered more than 100 scientific publications [42].

hydrogen [159, 161], or other point defects ( $V_{Ga} - V_N$ ) [148], thus leading to a number of other related energy levels between  $E_C - 1.2$  eV and  $E_C - 0.6$  eV.

Apart from the native defects, some extrinsic impurities, such as atoms that do not belong to the host matrix, can contaminate the GaN crystal. In some cases, the impurity incorporation is intentional (doping, compensation of the buffer layer, implantation for inter-device isolation, etc.) and can result in diffusion in unintended devices area; in other cases, the deep levels can be the result of chemical reactions involved in the crystal growth or processing.

One of the most severe sources of contamination is carbon, which is intentionally introduced in the buffer layers of HEMTs [162] to insulate the active layers of the devices from the substrate, or as a by-product from MOCVD [163, 164].

Carbon can form a substitutional defect on the nitrogen site ( $C_N$ ), which is responsible for the formation of a deep

acceptor theoretically located at  $E_V + 0.9$  eV [165], which found a wide agreement with experimental data [148, 166] and which may result in Fermi-level pinning rather than the release of free holes. In some references, it has been reported that C<sub>N</sub> forms a shallow acceptor-like level located at  $E_V + 0.13/0.3$  eV [157, 159, 161, 166–168]. It is worth noting that the carbon level is one of the main sources of trapping and  $R_{ON}$  instability in GaN HEMTs [6, 169]; often, activation energies around 0.3 eV have been reported. This is related to the transport by hopping of the holes between the carbon states, which are possibly clustered along dislocation lines [7], rather than a proper hole emission to the valence band.

Interstitial carbon defects (C<sub>I</sub>) are considered to induce a deep donor level with a typical activation energy around  $E_C - 1.25$  eV [161, 167].

Like carbon, iron doping has been widely employed to reduce the conductivity of UID GaN layers [170]. Fe is usually related to an acceptor deep level located at  $E_C - 0.6$  eV [171, 172], which is supported by experimental evidence from current collapse experiments in GaN HEMTs [8, 173].

Magnesium is the current standard doping species to obtain p-type conductivity in GaN, and forms a shallow deep level typically located between 0.15 eV and 0.2 eV above the valence band edge [174, 175]. Magnesium is also known to form complexes with hydrogen (Mg–H) tentatively located at  $E_C - 0.62$  eV [176] or  $E_C - 3.36$  eV [177], which are usually passivated during the activation of the dopant by RTA.

Hydrogen is a common contaminant resulting as a by-product of MOCVD growth. Because of the small atomic radius, it interacts with other defects including V<sub>Ga</sub> ( $E_C - 2.65$  eV) [159, 161] and C ( $E_C - 0.55$  eV) [178, 179].

Similarly to hydrogen, oxygen contaminants are likely to cluster with other defects, forming various deep levels approximately between  $E_C - 1.2$  eV and  $E_C - 0.4$  eV associated with V<sub>Ga</sub>–O [180] or O<sub>N</sub> [181].

## 8. Conclusions

In summary, in this topical review, we discussed the advancements in terms of defect spectroscopy in wide- and ultrawide-bandgap semiconductors. First, we showed that the interaction between electrons, photons, and phonons can be accurately described by the MPE model through the GCCD, which accounts for the displacement of the crystal lattice due to the different charge arrangements of the trapped and excited states. Then, we reviewed two spectroscopic techniques, C-DLTS and DLOS, with their advantages for the analysis of wide-bandgap semiconductors. After that, we presented a case study on the analysis of deep levels in nitrogen-implanted  $\beta$ -Ga<sub>2</sub>O<sub>3</sub> SBDs by means of DLOS, which showed the presence of two main traps, related to intrinsic point defects or their complex and nitrogen. In addition, we also proposed a methodology to adapt the DLOS analysis for use in wide- and ultra-wide-bandgap semiconductors.

Finally, we provided an overview of the most common traps in  $\beta$ -Ga<sub>2</sub>O<sub>3</sub> and GaN, which can serve as a reference for future studies.

## Data availability statement

The data that support the findings of this study are available upon reasonable request from the authors.

## Acknowledgments

This project has received funding from the ECSEL Joint Undertaking (JU) under Grant Agreement No. 101007229. The JU receives support from the European Union's Horizon 2020 Research and Innovation program and Germany, France, Belgium, Austria, Sweden, Spain, and Italy.

This work was partially supported by the GaN4AP Project—GaN for Advanced Power Applications, Project No. 101007310 funded by ECSEL Joint Undertaking.

This study was carried out within the MOST—Sustainable Mobility Center and received funding from the European Union NextGenerationEU (PIANO NAZIONALE DI RIPRESA E RESILIENZA (PNRR)—MISSIONE 4 COMPONENTE 2, INVESTIMENTO 1.4—D D 1033 17/06/2022, CN00000023). This manuscript reflects only the authors' views and opinions, and neither the European Union nor the European Commission can be considered responsible for them.

Project funded under the National Recovery and Resilience Plan (NRRP), Mission 4, Component C2, Investment 1.1, by the European Union—NextGenerationEU. PRIN Project 20225YYLEP, ‘Empowering UV LED technologies for high-efficiency disinfection: from semiconductor-level research to SARs-Cov-2 inactivation’.

## ORCID iDs

- Manuel Fregolent  <https://orcid.org/0000-0003-0801-2260>
- Francesco Piva  <https://orcid.org/0000-0003-3620-5510>
- Matteo Buffolo  <https://orcid.org/0000-0002-9255-6457>
- Carlo De Santi  <https://orcid.org/0000-0001-6064-077X>
- Andrea Cester  <https://orcid.org/0000-0001-6583-1735>
- Masataka Higashiwaki  <https://orcid.org/0000-0003-2821-3107>
- Gaudenzio Meneghesso  <https://orcid.org/0000-0002-6715-4827>
- Enrico Zanoni  <https://orcid.org/0000-0001-7349-9656>
- Matteo Meneghini  <https://orcid.org/0000-0003-2421-505X>

## References

- [1] Fregolent M, De Santi C, Buffolo M, Higashiwaki M, Meneghesso G, Zanoni E and Meneghini M 2021 Impact of thermal annealing on deep levels in nitrogen-implanted  $\beta$ -Ga<sub>2</sub>O<sub>3</sub> Schottky barrier diodes *J. Appl. Phys.* **130** 245704
- [2] De Santi C, Fregolent M, Buffolo M, Wong M H, Higashiwaki M, Meneghesso G, Zanoni E and Meneghini M 2020 Carrier capture kinetics, deep levels, and isolation properties of  $\beta$ -Ga<sub>2</sub>O<sub>3</sub> Schottky-barrier diodes damaged by nitrogen implantation *Appl. Phys. Lett.* **117** 262108

- [3] Greco G, Fiorenza P, Giannazzo F, Bongiorno C, Moschetti M, Bottari C, Alessandrino M S, Iucolano F and Roccaforte F 2022 Threshold voltage instability by charge trapping effects in the gate region of p-GaN HEMTs *Appl. Phys. Lett.* **121** 233506
- [4] Nicholls J R 2021 Electron trapping effects in SiC Schottky diodes: review and comment *Microelectron. Reliab.* **127** 114386
- [5] Florovič M, Škrinjarová J, Kováč J and Kordoš P 2016 Trapping analysis of AlGaN/GaN Schottky diodes via current transient spectroscopy *Electronics* **5** 20
- [6] Nardo A, De Santi C, Koller C, Ostermaier C, Daumiller I, Meneghesso G, Zanoni E and Meneghini M 2021 Positive and negative charge trapping GaN HEMTs: interplay between thermal emission and transport-limited processes *Microelectron. Reliab.* **126** 114255
- [7] Koller C, Pobegen G, Ostermaier C and Pogany D 2018 Effect of carbon doping on charging/discharging dynamics and leakage behavior of carbon-doped GaN *IEEE Trans. Electron Devices* **65** 5314–21
- [8] Cioni M, Zagni N, Selmi L, Meneghesso G, Meneghini M, Zanoni E and Chini A 2021 Electric field and self-heating effects on the emission time of iron traps in GaN HEMTs *IEEE Trans. Electron Devices* **68** 3325–32
- [9] Zagni N, Chini A, Puglisi F M, Meneghini M, Meneghesso G, Zanoni E, Pavan P and Verzellesi G 2021 “Hole Redistribution” model explaining the thermally activated RONStress/recovery transients in carbon-doped AlGaN/GaN power MIS-HEMTs *IEEE Trans. Electron Devices* **68** 697–703
- [10] Buffolo M, Caria A, Piva F, Roccato N, Casu C, De Santi C, Trivellin N, Meneghesso G, Zanoni E and Meneghini M 2022 Defects and reliability of GaN-Based LEDs: review and perspectives *Phys. Status Solidi a* **219** 2100727
- [11] Shockley W and Read W T 1952 Statistics of the Recombinations of Holes and Electrons *Phys. Rev.* **87** 835–42
- [12] Piva F *et al* 2023 Degradation of AlGaN-based UV-C SQW LEDs analyzed by means of capacitance deep-level transient spectroscopy and numerical simulations *Appl. Phys. Lett.* **122** 181102
- [13] Haller C, Carlin J-F, Jacquin G, Martin D, Butté R and Grandjean N 2017 Burying non-radiative defects in InGaN underlayer to increase InGaN/GaN quantum well efficiency *Appl. Phys. Lett.* **111** 262101
- [14] Armstrong A M, Crawford M H and Koleske D D 2014 Contribution of deep-level defects to decreasing radiative efficiency of InGaN/GaN quantum wells with increasing emission wavelength *Appl. Phys. Express* **7** 032101
- [15] Lin Y, Zhang Y, Guo Z, Zhang J, Huang W, Lu Y-J, Deng Z, Liu Z and Cao Y 2015 Defects dynamics during ageing cycles of InGaN blue light-emitting diodes revealed by evolution of external quantum efficiency—current dependence *Opt. Express* **23** A979
- [16] David A, Young N G, Lund C and Craven M D 2020 Review—the physics of recombinations in III-nitride emitters *ECS J. Solid State Sci. Technol.* **9** 016021
- [17] Trivellin N, Monti D, Piva F, Buffolo M, De Santi C, Zanoni E, Meneghesso G and Meneghini M 2019 Degradation processes of 280 nm high power DUV LEDs: impact on parasitic luminescence *Jpn. J. Appl. Phys.* **58** SCCC19
- [18] Reschchikov M A 2021 Measurement and analysis of photoluminescence in GaN *J. Appl. Phys.* **129** 121101
- [19] Ruschel J *et al* 2018 Localization of current-induced degradation effects in (InAlGa)N-based UV-B LEDs *J. Appl. Phys.* **124** 084504
- [20] Höpfner J *et al* 2023 Temperature-dependent electroluminescence of stressed and unstressed InAlGaN multi-quantum well UVB LEDs *Appl. Phys. Lett.* **122** 151104
- [21] Masin F, Meneghini M, Canato E, De Santi C, Stockman A, Zanoni E, Moens P and Meneghesso G 2019 Positive temperature dependence of time-dependent breakdown of GaN-on-Si E-mode HEMTs under positive gate stress *Appl. Phys. Lett.* **115** 052103
- [22] Tang S W *et al* 2022 Using gate leakage conduction to understand positive gate bias induced threshold voltage shift in p-GaN gate HEMTs *IEEE Trans. Electron Devices* **70** 449–53
- [23] Koller C, Pobegen G, Ostermaier C, Hecke G, Neumann R, Holzbauer M, Strasser G and Pogany D 2019 Trap-related breakdown and filamentary conduction in carbon doped GaN *Phys. Status. Solidi b* **256** 1800527
- [24] Roccato N *et al* 2023 Modeling the electrical degradation of AlGaN-based UV-C LEDs by combined deep-level optical spectroscopy and TCAD simulations *Appl. Phys. Lett.* **122** 161105
- [25] De Santi C, Buffolo M, Renzo N, Neviani A, Meneghesso G, Zanoni E and Meneghini M 2019 Evidence for defect-assisted tunneling and recombination at extremely low current in InGaN/GaN-based LEDs *Appl. Phys. Express* **12** 052007
- [26] Ruschel J, Glaab J, Beidoun B, Ploch N L, Rass J, Kolbe T, Knauer A, Weyers M, Einfeldt S and Kneissl M 2019 Current-induced degradation and lifetime prediction of 310 nm ultraviolet light-emitting diodes *Photon. Res.* **7** B36
- [27] Narendran N, Gu Y, Freyssinier J P, Yu H and Deng L 2004 Solid-state lighting: failure analysis of white LEDs *J. Cryst. Growth* **268** 449–56
- [28] Kwon W, Kawasaki S, Watanabe H, Tanaka A, Honda Y, Ikeda H, Iso K and Amano H 2023 Reverse leakage mechanism of dislocation-free GaN vertical p-n diodes *IEEE Electron Device Lett.* **44** 1172–5
- [29] Lang D V 1974 Deep-level transient spectroscopy: a new method to characterize traps in semiconductors *J. Appl. Phys.* **45** 3023–32
- [30] Barbolla J, Dueñas S and Bailón L 1992 Admittance spectroscopy in junctions *Solid State Electron.* **35** 285–97
- [31] Chantre A, Vincent G and Bois D 1981 Deep-level optical spectroscopy in GaAs *Phys. Rev. B* **23** 5335–59
- [32] Isoya J, Umeda T, Mizuuchi N, Son N T, Janzén E and Ohshima T 2008 EPR identification of intrinsic defects in SiC *Phys. Status Solidi b* **245** 1298–314
- [33] Wang X, Xu Z, Rommel M, Dong B, Song L, Tee C A T and Fang F 2019 Electron paramagnetic resonance characterization of aluminum ion implantation-induced defects in 4H-SiC *Nanotechnol. Precis. Eng.* **2** 157–62
- [34] Amano H, Kito M, Hiramatsu K and Akasaki I 1989 P-type conduction in Mg-doped GaN treated with low-energy electron beam irradiation (LEEBI) *Jpn. J. Appl. Phys.* **28** L2112
- [35] Schubert E F 2006 *Light-Emitting Diodes* (Cambridge University Press)
- [36] Amano H *et al* 2020 The 2020 UV emitter roadmap *J. Phys. D: Appl. Phys.* **53** 503001
- [37] Vasilopoulou M, Fakharuddin A, García de Arquer F P, Georgiadou D G, Kim H, Mohd Yusoff Abd R B, Gao F, Nazeeruddin M K, Bolink H J and Sargent E H 2021 Advances in solution-processed near-infrared light-emitting diodes *Nat. Photon.* **15** 656–69
- [38] Auf der Maur M, Pecchia A, Penazzi G, Rodrigues W and Di Carlo A 2016 Efficiency drop in green InGaN/GaN light emitting diodes: the role of random alloy fluctuations *Phys. Rev. Lett.* **116** 027401

- [39] Mishra U K, Parikh P and Wu Y-F 2002 AlGaN/GaN HEMTs—an overview of device operation and applications *Proc. IEEE* **90** 1022–31
- [40] Hoo Teo K, Zhang Y, Chowdhury N, Rakheja S, Ma R, Xie Q, Yagyu E, Yamamoto K, Li K and Palacios T 2021 Emerging GaN technologies for power, RF, digital, and quantum computing applications: recent advances and prospects *J. Appl. Phys.* **130** 160902
- [41] Zanoni E *et al* 2023 Microwave and millimeter-wave GaN HEMTs: impact of epitaxial structure on short-channel effects, electron trapping, and reliability *IEEE Trans. Electron Devices* **71** 1396–407
- [42] Meneghini M *et al* 2021 GaN-based power devices: physics, reliability, and perspectives *J. Appl. Phys.* **130** 181101
- [43] Chowdhury S and Ji D 2020 Vertical GaN power devices *Nitride Semiconductor Technology* (Wiley) pp 177–97
- [44] Nie H, Diduck Q, Alvarez B, Edwards A P, Kayes B M, Zhang M, Ye G, Prunty T, Bour D and Kizilyalli I C 2014 1.5 kV and 2.2 mΩ cm<sup>2</sup> vertical GaN transistors on bulk-GaN substrates *IEEE Electron Device Lett.* **35** 939–41
- [45] Liu J, Xiao M, Zhang Y, Pidaparthi S, Cui H, Edwards A, Baubut L, Meier W, Coles C and Drowley C 2020 1.2 kV vertical GaN Fin JFETs with robust avalanche and fast switching capabilities *Technical Digest—Int. Electron Devices Meeting, IEDM* vol 2020 pp 23.2.1–23.2.4
- [46] Higashiwaki M, Sasaki K, Kuramata A, Masui T and Yamakoshi S 2012 Gallium oxide ( $\text{Ga}_2\text{O}_3$ ) metal-semiconductor field-effect transistors on single-crystal  $\beta$ - $\text{Ga}_2\text{O}_3$  (010) substrates *Appl. Phys. Lett.* **100** 013504
- [47] Green A J *et al* 2022  $\beta$ -Gallium oxide power electronics *APL Mater.* **10** 029201
- [48] Higashiwaki M 2021  $\beta$ -gallium oxide devices: progress and outlook *Phys. Status Solidi* **15** 2100357
- [49] Lv Y *et al* 2020 Lateral  $\beta$ - $\text{Ga}_2\text{O}_3$  MOSFETs with high power figure of merit of 277 MW/cm<sup>2</sup> *IEEE Electron Device Lett.* **41** 537–40
- [50] Tetzner K, Bahat Treidel E, Hilt O, Popp A, Bin Anooz S, Wagner G, Thies A, Ickert K, Gargouri H and Wurfl J 2019 Lateral 1.8 kV  $\beta$ - $\text{Ga}_2\text{O}_3$  MOSFET With 155 MW/cm<sup>2</sup> power figure of merit *IEEE Electron Device Lett.* **40** 1503–6
- [51] Tetzner K *et al* 2022 SnO/ $\beta$ - $\text{Ga}_2\text{O}_3$  heterojunction field-effect transistors and vertical p–n diodes *Appl. Phys. Lett.* **120** 112110
- [52] Bhattacharyya A, Ranga P, Roy S, Peterson C, Alema F, Serygin G, Osinsky A and Krishnamoorthy S 2021 Multi-kV Class  $\beta$ - $\text{Ga}_2\text{O}_3$  MESFETs with a lateral figure of merit up to 355 MW/cm<sup>2</sup> *IEEE Electron Device Lett.* **42** 1272–5
- [53] Higashiwaki M, Wong M H, Goto K, Murakami H and Kumagai Y 2020 Vertical gallium oxide transistors with current aperture formed using nitrogen-ion implantation process *2020 4th IEEE Electron Devices Technology & Manufacturing Conf. (EDTM)* (IEEE) pp 1–3
- [54] Hu Z, Nomoto K, Li W, Jinno R, Nakamura T, Jena D and Xing H 2019 1.6 kV vertical  $\text{Ga}_2\text{O}_3$  FinFETs with source-connected field plates and normally-off operation *2019 31st Int. Symp. on Power Semiconductor Devices and ICs (ISPSD)* vol 2019 (IEEE) pp 483–6
- [55] Chen X, Li F and Hess H L 2023 Trench gate  $\beta$ - $\text{Ga}_2\text{O}_3$  MOSFETs: a review *Eng. Res. Express* **5** 012004
- [56] Yadava N and Chauhan R K 2020 Review—recent advances in designing gallium oxide MOSFET for RF application *ECS J. Solid State Sci. Technol.* **9** 065010
- [57] Kaur D and Kumar M 2021 A strategic review on gallium oxide based deep-ultraviolet photodetectors: recent progress and future prospects *Adv. Opt. Mater.* **9** 2002160
- [58] Chen X, Ren F, Gu S and Ye J 2019 Review of gallium-oxide-based solar-blind ultraviolet photodetectors *Photon. Res.* **7** 381
- [59] Higashiwaki M and Jessen G H 2018 Guest editorial: the dawn of gallium oxide microelectronics *Appl. Phys. Lett.* **112** 060401
- [60] Jamwal N S and Kiani A 2022 Gallium oxide nanostructures: a review of synthesis, properties and applications *Nanomaterials* **12** 2061
- [61] Stepanov S I, Nikolaev V I, Bougov V E and Romanov A E 2016 Gallium oxide: properties and applications—A review *Rev. Adv. Mater. Sci.* **44** 63–86
- [62] Moser N, Liddy K, Islam A, Miller N, Leedy K, Asel T, Mou S, Green A and Chabak K 2020 Toward high voltage radio frequency devices in  $\beta$ - $\text{Ga}_2\text{O}_3$  *Appl. Phys. Lett.* **117** 242101
- [63] Bai J, Yang C C, Athanasiou M and Wang T 2014 Efficiency enhancement of InGaN/GaN solar cells with nanostructures *Appl. Phys. Lett.* **104** 051129
- [64] Rockett A 2008 *The Materials Science of Semiconductors* vol 19 (Springer)
- [65] Hall R N 1952 Electron-hole recombination in germanium *Phys. Rev.* **87** 387
- [66] Schroder D K 2005 *Semiconductor Material and Device Characterization* (John Wiley & Sons, Inc.)
- [67] Ruch B, Jech M, Pobegen G and Grasser T 2020 Applicability of Shockley-Read-Hall theory for interface states *Technical Digest—Int. Electron Devices Meeting, IEDM* vol 2020 (Institute of Electrical and Electronics Engineers Inc.) pp 22.1.1–22.1.4
- [68] Fregolent M, Buffolo M, De Santi C, Hasegawa S, Matsumura J, Nishinaka H, Yoshimoto M, Meneghini M 2021 Deep levels and carrier capture kinetics in n-GaAsBi alloys investigated by deep level transient spectroscopy *J. Appl. Phys.* **54** 345109
- [69] Mooney P M 1999 Chapter 2 defect identification using capacitance spectroscopy *Semicond. Semimet.* **51** 93–152
- [70] Henry C H and Lang D V 1977 Nonradiative capture and recombination by multiphonon emission in GaAs and GaP *Phys. Rev. B* **15** 989–1016
- [71] Pässler R 1978 Temperature dependences of the nonradiative multiphonon carrier capture and ejection properties of deep traps in semiconductors. I. Theoretical results *Phys. Status Solidi b* **85** 203–15
- [72] Alkauskas A, McCluskey M D and Van De Walle C G 2016 Tutorial: defects in semiconductors—Combining experiment and theory *J. Appl. Phys.* **119** 181101
- [73] Lax M 1952 The Franck-Condon principle and its application to crystals *J. Chem. Phys.* **20** 1752–60
- [74] Alkauskas A, Yan Q and Van De Walle C G 2014 First-principles theory of nonradiative carrier capture via multiphonon emission *Phys. Rev. B* **90** 075202
- [75] Ganichev S D, Prettl W and Yassievich I N 1997 Deep impurity-center ionization by far-infrared radiation *Phys. Solid State* **39** 1703–26
- [76] Anon 1950 Theory of light absorption and non-radiative transitions in F-centres *Proc. R. Soc. A* **204** 406–23
- [77] Wang Z, Chen X, Ren F-F, Gu S and Ye J 2021 Deep-level defects in gallium oxide *J. Appl. Phys.* **54** 043002
- [78] Auret F D *et al* 2007 Electronic properties of defects in pulsed-laser deposition grown ZnO with levels at 300 and 370 meV below the conduction band *Physica B* **401–402** 378–81
- [79] Wosiński T 1989 Evidence for the electron traps at dislocations in GaAs crystals *J. Appl. Phys.* **65** 1566–70

- [80] Omling P, Weber E R, Montelius L, Alexander H and Michel J 1985 Electrical properties of dislocations and point defects in plastically deformed silicon *Phys. Rev. B* **32** 6571–81
- [81] Modolo N, De Santi C, Minetto A, Sayadi L, Prechtl G, Meneghesso G, Zanoni E and Meneghini M 2022 Trap-state mapping to model GaN transistors dynamic performance *Sci. Rep.* **12** 1–10
- [82] Schröter W, Kronewitz J, Gnauert U, Riedel F and Seibt M 1995 Bandlike and localized states at extended defects in silicon *Phys. Rev. B* **52** 13726–9
- [83] Hierro A, Arehart A R R, Heying B, Hansen M, Speck J S S, Mishra U K K, DenBaars S P P and Ringel S A A 2001 Capture kinetics of electron traps in MBE-Grown n-GaN *Phys. Status Solidi b* **228** 309–13
- [84] Wessels B W 1976 Determination of deep levels in Cu-doped GaP using transient-current spectroscopy *J. Appl. Phys.* **47** 1131–3
- [85] Borsuk J A and Swanson R M 1980 Current transient spectroscopy: a high-sensitivity DLTS system *IEEE Trans. Electron Devices* **27** 2217–25
- [86] Lefèvre H and Schulz M 1977 Double correlation technique (DDLTS) for the analysis of deep level profiles in semiconductors *Appl. Phys.* **12** 45–53
- [87] Peaker A R, Markevich V P and Coutinho J 2018 Junction spectroscopy techniques and deep-level defects in semiconductors *J. Appl. Phys.* **123** 161559
- [88] Goto G, Yanagisawa S, Wada O and Takanashi H 1974 An improved method of determining deep impurity levels and profiles in semiconductors *Jpn. J. Appl. Phys.* **13** 1127–33
- [89] Pals J A 1974 Properties of Au, Pt, Pd and Rh levels in silicon measured with a constant capacitance technique *Solid State Electron.* **17** 1139–45
- [90] Engemann J and Heime K 1975 Deep-impurity-level spectroscopy at the GaAs epilayer/substrate interface, using a new constant-capacitance TSCAP method *C R C Crit. Rev. Solid State Sci.* **5** 485–9
- [91] Johnson N M 1982 Measurement of semiconductor–insulator interface states by constant-capacitance deep-level transient spectroscopy *J. Vac. Sci. Technol.* **21** 303–14
- [92] Basile A F, Rozen J, Williams J R, Feldman L C and Mooney P M 2011 Capacitance-voltage and deep-level-transient spectroscopy characterization of defects near SiO<sub>2</sub>/SiC interfaces *J. Appl. Phys.* **109** 064514
- [93] Afanasev V V, Stesmans A, Bassler M, Pensl G and Schulz M J 2000 Shallow electron traps at the 4H-SiC/SiO<sub>2</sub> interface *Appl. Phys. Lett.* **76** 336–8
- [94] Johnson N M, Bartelink D J, Gold R B and Gibbons J F 1979 Constant-capacitance DLTS measurement of defect-density profiles in semiconductors *J. Appl. Phys.* **50** 4828–33
- [95] Whight K R 1982 Junction structure effects on constant capacitance DLTS and ODLTS spectra *Solid State Electron.* **25** 893–901
- [96] Kowaki H, Lee K-H, Kojima T, Inagaki M, Ikeda K, Bouzazi B, Kojima N, Ohshita Y, Yamaguchi M and Ekins-Daukes N J 2013 Optical DLTS for the study of recombination centers in GaAsN grown by chemical beam epitaxy *AIP Conf. Proc.* **1556** 41–44
- [97] Furukawa Y 1967 Trap levels in gallium arsenide *Jpn. J. Appl. Phys.* **6** 675
- [98] Sah C T, Forbes L, Rosier L L and Tasch A F 1970 Thermal and optical emission and capture rates and cross sections of electrons and holes at imperfection centers in semiconductors from photo and dark junction current and capacitance experiments *Solid State Electron.* **13** 759–88
- [99] Pässler R 2004 Photoionization cross-section analysis for a deep trap contributing to current collapse in GaN field-effect transistors *J. Appl. Phys.* **96** 715–22
- [100] Lucovsky G 1965 On the photoionization of deep impurity centers in semiconductors *Solid State Commun.* **3** 299–302
- [101] Fregolent M, Del Fiò A, De Santi C, Huber C, Meneghesso G, Zanoni E and Meneghini M 2023 Threshold voltage instability in SiO<sub>2</sub>-gate semi-vertical GaN trench MOSFETs grown on silicon substrate *Microelectron. Reliab.* **150** 115130
- [102] Favero D *et al* 2023 High-temperature PBTI in trench-gate vertical GaN power MOSFETs: role of border and semiconductor traps *IEEE Int. Reliability Physics Symp. Proc.* vol 2023 (Institute of Electrical and Electronics Engineers Inc.)
- [103] Zheng Z *et al* 2021 Threshold voltage instability of enhancement-mode GaN buried p-channel MOSFETs *IEEE Electron Device Lett.* **42** 1584–7
- [104] Stockman A, Canato E, Meneghini M, Meneghesso G, Moens P and Bakeroot B 2019 Threshold voltage instability mechanisms in p-GaN gate AlGaN/GaN HEMTs 2019 31st Int. Symp. on Power Semiconductor Devices and ICs (ISPSD) (IEEE) pp 287–90
- [105] Meneghesso G, Meneghini M, De Santi C, Ruzzarin M and Zanoni E 2018 Positive and negative threshold voltage instabilities in GaN-based transistors *Microelectron. Reliab.* **80** 257–65
- [106] Fregolent M, Brusaterra E, De Santi C, Tetzner K, Würfl J, Meneghesso G, Zanoni E and Meneghini M 2022 Logarithmic trapping and detrapping in β-Ga<sub>2</sub>O<sub>3</sub> MOSFETs: experimental analysis and modelling *Appl. Phys. Lett.* **120** 163502
- [107] Wolters D R and van der Schoot J J 1985 Kinetics of charge trapping in dielectrics *J. Appl. Phys.* **58** 831–7
- [108] Meneghini M, Rossetto I, Bisi D, Stocco A, Chini A, Pantellini A, Lanzieri C, Nanni A, Meneghesso G and Zanoni E 2014 Buffer traps in Fe-doped AlGaN/GaN HEMTs: investigation of the physical properties based on pulsed and transient measurements *IEEE Trans. Electron Devices* **61** 4070–7
- [109] Modolo N, De Santi C, Minetto A, Sayadi L, Sicre S, Prechtl G, Meneghesso G, Zanoni E and Meneghini M 2021 A physics-based approach to model hot-electron trapping kinetics in p-GaN HEMTs *IEEE Electron Device Lett.* **42** 673–6
- [110] Modolo N, Tang S, Jiang H, De Santi C, Meneghini M and Wu T-L 2021 A novel physics-based approach to analyze and model E-mode p-GaN power HEMTs *IEEE Trans. Electron Devices* **68** 1489–94
- [111] Wong M H, Lin C H, Kuramata A, Yamakoshi S, Murakami H, Kumagai Y and Higashiwaki M 2018 Acceptor doping of β-Ga<sub>2</sub>O<sub>3</sub> by Mg and N ion implantations *Appl. Phys. Lett.* **113** 102103
- [112] Ghadi H *et al* 2023 Identification and characterization of deep nitrogen acceptors in β-Ga<sub>2</sub>O<sub>3</sub> using defect spectroscopies *APL Mater.* **11** 111110
- [113] Irmscher K, Galazka Z, Pietsch M, Uecker R and Fornari R 2011 Electrical properties of β-Ga<sub>2</sub>O<sub>3</sub> single crystals grown by the Czochralski method *J. Appl. Phys.* **110** 063720
- [114] Ingebrigtsen M E, Varley J B, Kuznetsov A Y, Svensson B G, Alfieri G, Mihaila A, Badstübler U and Vines L 2018 Iron and intrinsic deep level states in Ga<sub>2</sub>O<sub>3</sub> *Appl. Phys. Lett.* **112** 042104
- [115] Zhang Z, Farzana E, Arehart A R and Ringel S A 2016 Deep level defects throughout the bandgap of (010) β-Ga<sub>2</sub>O<sub>3</sub> detected by optically and thermally stimulated defect spectroscopy *Appl. Phys. Lett.* **108** 2–7

- [116] Polyakov A Y, Smirnov N B, Shchemerov I V, Yakimov E B, Yang J, Ren F, Yang G, Kim J, Kuramata A and Pearton S J 2018 Point defect induced degradation of electrical properties of  $\text{Ga}_2\text{O}_3$  by 10 MeV proton damage *Appl. Phys. Lett.* **112** 032107
- [117] Polyakov A Y *et al* 2018 Defects responsible for charge carrier removal and correlation with deep level introduction in irradiated  $\beta\text{-Ga}_2\text{O}_3$  *Appl. Phys. Lett.* **113** 092102
- [118] Farzana E, Chaiken M F, Blue T E, Arehart A R and Ringel S A 2019 Impact of deep level defects induced by high energy neutron radiation in  $\beta\text{-Ga}_2\text{O}_3$  *APL Mater.* **7** 022502
- [119] McGlone J F, Xia Z, Zhang Y, Joishi C, Lodha S, Rajan S, Ringel S A and Arehart A R 2018 Trapping effects in Si-doped  $\text{Ga}_2\text{O}_3$  MESFETs on an Fe-doped  $\text{Ga}_2\text{O}_3$  Substrate *IEEE Electron Device Lett.* **39** 1042–5
- [120] Zimmermann C, Frdestrom Verhoeven E, Kalman Fradason Y, Weiser P M, Varley J B and Vines L 2020 Formation and control of the  $E^*2$  center in implanted  $\beta\text{-Ga}_2\text{O}_3$  by reverse-bias and zero-bias annealing *J. Phys. D: Appl. Phys.* **53** 464001
- [121] Polyakov A Y, Smirnov N B, Shchemerov I V, Gogova D, Tarelkin S A and Pearton S J 2018 Compensation and persistent photocapacitance in homoepitaxial Sn-doped  $\beta\text{-Ga}_2\text{O}_3$  *J. Appl. Phys.* **123** 115702
- [122] Ghadi H, McGlone J F, Cornuelle E, Feng Z, Zhang Y, Meng L, Zhao H, Arehart A R and Ringel S A 2022 Deep level defects in low-pressure chemical vapor deposition grown (010)  $\beta\text{-Ga}_2\text{O}_3$  *APL Mater.* **10** 101110
- [123] Ghadi H, McGlone J F, Feng Z, Bhuiyan A F M A U, Zhao H, Arehart A R and Ringel S A 2020 Influence of growth temperature on defect states throughout the bandgap of MOCVD-grown  $\beta\text{-Ga}_2\text{O}_3$  *Appl. Phys. Lett.* **117** 172106
- [124] Kuramata A, Koshi K, Watanabe S, Yamaoka Y, Masui T and Yamakoshi S 2016 High-quality  $\beta\text{-Ga}_2\text{O}_3$  single crystals grown by edge-defined film-fed growth *Jpn. J. Appl. Phys.* **55** 1202A2
- [125] Bhandari S and Zvanut M E 2021 Charge trapping at Fe due to midgap levels in  $\text{Ga}_2\text{O}_3$  *J. Appl. Phys.* **129** 085703
- [126] Zimmermann C, Fradason Y K, Barnard A W, Varley J B, Irmscher K, Galazka Z, Karjalainen A, Meyer W E, Auret F D and Vines L 2020 Ti-A nd Fe-related charge transition levels in  $\beta\text{-Ga}_2\text{O}_3$  *Appl. Phys. Lett.* **116** 072101
- [127] McGlone J F, Xia Z, Joishi C, Lodha S, Rajan S, Ringel S and Arehart A R 2019 Identification of critical buffer traps in Si doped  $\beta\text{-Ga}_2\text{O}_3$  MESFETs *Appl. Phys. Lett.* **115** 153501
- [128] Ingebrigtsen M E, Kuznetsov A Y, Svensson B G, Alfieri G, Mihaila A, Badstüber U, Perron A, Vines L and Varley J B 2019 Impact of proton irradiation on conductivity and deep level defects in  $\beta\text{-Ga}_2\text{O}_3$  *APL Mater.* **7** 022510
- [129] Polyakov A Y *et al* 2021 1 GeV proton damage in  $\beta\text{-Ga}_2\text{O}_3$  *J. Appl. Phys.* **130** 185701
- [130] Farzana E, Ahmadi E, Speck J S, Arehart A R and Ringel S A 2018 Deep level defects in Ge-doped (010)  $\beta\text{-Ga}_2\text{O}_3$  layers grown by plasma-assisted molecular beam epitaxy *J. Appl. Phys.* **123** 161410
- [131] Ghadi H, McGlone J F, Jackson C M, Farzana E, Feng Z, Bhuiyan A F M A U, Zhao H, Arehart A R and Ringel S A 2020 Full bandgap defect state characterization of  $\beta\text{-Ga}_2\text{O}_3$  grown by metal organic chemical vapor deposition *APL Mater.* **8** 21111
- [132] McGlone J F, Ghadi H, Cornuelle E, Armstrong A, Burns G, Feng Z, Uddin Bhuiyan A F M A, Zhao H, Arehart A R and Ringel S A 2023 Proton radiation effects on electronic defect states in MOCVD-grown (010)  $\beta\text{-Ga}_2\text{O}_3$  *J. Appl. Phys.* **133** 045702
- [133] Armstrong A M, Crawford M H, Jayawardena A, Ahyi A and Dhar S 2016 Role of self-trapped holes in the photoconductive gain of  $\beta$ -gallium oxide Schottky diodes *J. Appl. Phys.* **119** 1–7
- [134] Polyakov A Y, Smirnov N B, Shchemerov I V, Pearton S J, Ren F, Chernykh A V, Lagov P B and Kulevoy T V 2018 Hole traps and persistent photocapacitance in proton irradiated  $\beta\text{-Ga}_2\text{O}_3$  films doped with Si *APL Mater.* **6** 096102
- [135] Wang Z *et al* 2022 Majority and minority carrier traps in  $\text{NiO}/\beta\text{-Ga}_2\text{O}_3\text{p}+\text{n}$  heterojunction diode *IEEE Trans. Electron Devices* **69** 981–7
- [136] Neal A T, Mou S, Lopez R, Li J V, Thomson D B, Chabak K D and Jessen G H 2017 Incomplete ionization of a 110 meV unintentional donor in  $\beta\text{-Ga}_2\text{O}_3$  and its effect on power devices *Sci. Rep.* **7** 13218
- [137] Wong M H and Higashiwaki M 2019 Gallium oxide field effect transistors—establishing new frontiers of power switching and radiation-hard electronics *Int. J. High Speed Electron. Syst.* **28** 1940002
- [138] Asghar M, Muret P, Beaumont B and Gibart P 2004 Field dependent transformation of electron traps in GaN p-n diodes grown by metal-organic chemical vapour deposition *Mater. Sci. Eng. B* **113** 248–52
- [139] Boturchuk I, Scheffler L, Larsen A N and Julsgaard B 2018 Evolution of electrically active defects in n-GaN during heat treatment typical for ohmic contact formation *Phys. Status Solidi a* **215** 1700516
- [140] Zhang Z, Arehart A R, Kyle E C H, Chen J, Zhang E X, Fleetwood D M, Schrimpf R D, Speck J S and Ringel S A 2015 Proton irradiation effects on deep level states in Mg-doped p-type GaN grown by ammonia-based molecular beam epitaxy *Appl. Phys. Lett.* **106** 173504
- [141] Polyakov A Y, Smirnov N B, Turutin A V, Shemerov I S, Ren F, Pearton S J and Johnson J W 2016 Deep traps and instabilities in AlGaN/GaN high electron mobility transistors on Si substrates *J. Vac. Sci. Technol. B* **34** 041216
- [142] Cho H K, Kim C S and Hong C-H 2003 Electron capture behaviors of deep level traps in unintentionally doped and intentionally doped n-type GaN *J. Appl. Phys.* **94** 1485–9
- [143] Cho H K, Kim K S, Hong C-H and Lee H J 2001 Electron traps and growth rate of buffer layers in unintentionally doped GaN *J. Cryst. Growth* **223** 38–42
- [144] Cho H K, Khan F A, Adesida I, Fang Z-Q and Look D C 2008 Deep level characteristics in n-GaN with inductively coupled plasma damage *J. Phys. D: Appl. Phys.* **41** 155314
- [145] Arehart A R, Homan T, Wong M H, Poblenz C, Speck J S and Ringel S A 2010 Impact of N- and Ga-face polarity on the incorporation of deep levels in n-type GaN grown by molecular beam epitaxy *Appl. Phys. Lett.* **96** 242112
- [146] Chen S, Honda U, Shibata T, Matsumura T, Tokuda Y, Ishikawa K, Hori M, Ueda H, Uesugi T and Kachi T 2012 As-grown deep-level defects in n-GaN grown by metal-organic chemical vapor deposition on freestanding GaN *J. Appl. Phys.* **112** 053513
- [147] Park Y S, Lee M, Jeon K, Yoon I T, Shon Y, Im H, Park C J, Cho H Y and Han M-S 2010 Deep level transient spectroscopy in plasma-assisted molecular beam epitaxy grown  $\text{Al}_{0.2}\text{Ga}_{0.8}\text{N}/\text{GaN}$  interface and the rapid thermal annealing effect *Appl. Phys. Lett.* **97** 112110
- [148] Honda U, Yamada Y, Tokuda Y and Shiojima K 2012 Deep levels in n-GaN doped with carbon studied by deep level and minority carrier transient spectroscopies *Jpn. J. Appl. Phys.* **51** 04DF04
- [149] Umana-Membreno G A, Dell J M, Hessler T P, Nener B D, Parish G, Faraone L and Mishra U K 2002 60Co gamma-irradiation-induced defects in n-GaN *Appl. Phys. Lett.* **80** 4354–6

- [150] Hullavarad S S, Bhoraskar S V, Sainkar S R, Badrinarayanan S, Mandale A B and Ganeshan V 1999 Deep levels in GaN grown by nitridation of GaAs (110) surface in a electron cyclotron}resonance ammonia plasma *Vacuum* **55** 121–6
- [151] Johnstone D, Ahoujjab M, Yeob Y K and Guidoc L 2001 GaN deep level capture barriers *Proc. SPIE* **4288** 209–18
- [152] Kojima K, Takashima S, Edo M, Ueno K, Shimizu M, Takahashi T, Ishibashi S, Uedono A and Chichibu S F 2017 Nitrogen vacancies as a common element of the green luminescence and nonradiative recombination centers in Mg-implanted GaN layers formed on a GaN substrate *Appl. Phys. Express* **10** 061002
- [153] Yan Q, Janotti A, Scheffler M and Van De Walle C G 2012 Role of nitrogen vacancies in the luminescence of Mg-doped GaN *Appl. Phys. Lett.* **100** 142110
- [154] Li F, Liu J, Tian A, Li X, Zhang F and Yang H 2023 Nitrogen vacancies in GaN templates and their critical role on the luminescence efficiency of blue quantum wells *Opt. Express* **31** 14937
- [155] Hacke P, Detchprohm T, Hiramatsu K, Sawaki N, Tadatomo K and Miyake K 1994 Analysis of deep levels in *n*-type GaN by transient capacitance methods *J. Appl. Phys.* **76** 304–9
- [156] Chung H M, Chuang W C, Pan Y C, Tsai C C, Lee M C, Chen W H, Chen W K, Chiang C I, Lin C H and Chang H 2000 Electrical characterization of isoelectronic In-doping effects in GaN films grown by metalorganic vapor phase epitaxy *Appl. Phys. Lett.* **76** 897–9
- [157] Hierro A, Arehart A R, Heying B, Hansen M, Mishra U K, Denbaars S P, Speck J S and Ringel S A 2002 Impact of Ga/N flux ratio on trap states in n-GaN grown by plasma-assisted molecular-beam epitaxy *Appl. Phys. Lett.* **80** 805–7
- [158] Calleja E *et al* 1997 Yellow luminescence and related deep states in undoped GaN *Phys. Rev. B* **55** 4689–94
- [159] Zhang Z, Hurni C A, Arehart A R, Yang J, Myers R C, Speck J S and Ringel S A 2012 Deep traps in nonpolar *m*-plane GaN grown by ammonia-based molecular beam epitaxy *Appl. Phys. Lett.* **100** 052114
- [160] Belahsene S, Al Saqri N, Jameel D, Mesli A, Martinez A, de Sanoit J, Ougazzaden A, Salvestrini J, Ramdane A and Henini M 2015 Analysis of deep level defects in GaN p-i-n diodes after beta particle irradiation *Electronics* **4** 1090–100
- [161] Arehart A R, Corrion A, Poblenz C, Speck J S, Mishra U K, DenBaars S P and Ringel S A 2008 Comparison of deep level incorporation in ammonia and rf-plasma assisted molecular beam epitaxy n-GaN films *Phys. Status Solidi c* **5** 1750–2
- [162] Bahat-Treidel E, Brunner F, Hilt O, Cho E, Würfl J and Trankle G 2010 AlGaN/GaN/GaN:C back-barrier HFETs with breakdown voltage of over 1 kV and low RON × A *IEEE Trans. Electron Devices* **57** 3050–8
- [163] Fabris E *et al* 2020 Impact of residual carbon on avalanche voltage and stability of polarization-induced vertical GaN p-n junction *IEEE Trans. Electron Devices* **67** 3978–82
- [164] He X G *et al* 2014 Control of residual carbon concentration in GaN high electron mobility transistor and realization of high-resistance GaN grown by metal-organic chemical vapor deposition *Thin Solid Films* **564** 135–9
- [165] Lyons J L, Janotti A and Van De Walle C G 2014 Effects of carbon on the electrical and optical properties of InN, GaN, and AlN *Phys. Rev. B* **89** 035204
- [166] Lee I-H, Polyakov A Y, Smirnov N B, Zinovyev R A, Bae K-B, Chung T-H, Hwang S-M, Baek J H and Pearton S J 2017 Changes in electron and hole traps in GaN-based light emitting diodes from near-UV to green spectral ranges *Appl. Phys. Lett.* **110** 192107
- [167] Nguyen X S, Hou H W, De Mierry P, Vennéguès P, Tendille F, Arehart A R, Ringel S A, Fitzgerald E A and Chua S J 2016 Deep level traps in semi-polar n-GaN grown on patterned sapphire substrate by metalorganic vapor phase epitaxy *Phys. Status Solidi b* **253** 2225–9
- [168] Narita T, Tomita K, Tokuda Y, Kogiso T, Horita M and Kachi T 2018 The origin of carbon-related carrier compensation in p-type GaN layers grown by MOVPE *J. Appl. Phys.* **124** 215701
- [169] Meneghini M, Tajalli A, Moens P, Banerjee A, Zanoni E and Meneghesso G 2018 Trapping phenomena and degradation mechanisms in GaN-based power HEMTs *Mater. Sci. Semicond. Process.* **78** 118–26
- [170] Silvestri M, Uren M J and Kuball M 2013 Iron-induced deep-level acceptor center in GaN/AlGaN high electron mobility transistors: energy level and cross section *Appl. Phys. Lett.* **102** 073501
- [171] Horita M, Narita T, Kachi T and Suda J 2020 Identification of origin of E C-0.6 eV electron trap level by correlation with iron concentration in n-type GaN grown on GaN freestanding substrate by metalorganic vapor phase epitaxy *Appl. Phys. Express* **13** 071007
- [172] Sharma K, Dupouy E, Bouslama M, Sommet R and Nallatamby J-C 2020 Impact of the location of iron buffer doping on trap signatures in GaN HEMTs 2020 *Int. Workshop on Integrated Nonlinear Microwave and Millimetre-Wave Circuits (Innmic)* (IEEE) pp 1–3
- [173] Cardwell D W, Sasikumar A, Arehart A R, Kaun S W, Lu J, Keller S, Speck J S, Mishra U K, Ringel S A and Pelz J P 2013 Spatially-resolved spectroscopic measurements of Ec—0.57 eV traps in AlGaN/GaN high electron mobility transistors *Appl. Phys. Lett.* **102** 193509
- [174] Tanaka T, Watanabe A, Amano H, Kobayashi Y, Akasaki I, Yamazaki S and Koike M 1994 P-type conduction in Mg-doped GaN and Al<sub>0.08</sub>Ga<sub>0.92</sub>N grown by metalorganic vapor phase epitaxy *Appl. Phys. Lett.* **65** 593–4
- [175] Nakayama H, Hacke P, Khan M R H, Detchprohm T, Kazumasa Hiramatsu K H and Nobuhiko Sawaki N S 1996 Electrical transport properties of p-GaN *Jpn. J. Appl. Phys.* **35** L282
- [176] Kogiso T, Narita T, Tokuda Y, Tomita K and Kachi T 2019 Characterization of hole traps in MOVPE-grown p-type GaN layers using low-frequency capacitance deep-level transient spectroscopy *Jpn. J. Appl. Phys.* **58** SCCC36
- [177] Hierro A, Ringel S A, Hansen M, Speck J S, Mishra U K and DenBaars S P 2000 Hydrogen passivation of deep levels in n-GaN *Appl. Phys. Lett.* **77** 1499–501
- [178] Wang C D, Yu L S, Lau S S, Yu E T, Kim W, Botchkarev A E and Morkoç H 1998 Deep level defects in *n*-type GaN grown by molecular beam epitaxy *Appl. Phys. Lett.* **72** 1211–3
- [179] Lee W I, Huang T C, Guo J D and Feng M S 1995 Effects of column III alkyl sources on deep levels in GaN grown by organometallic vapor phase epitaxy *Appl. Phys. Lett.* **67** 1721–3
- [180] Stuchlikova L *et al* 2010 Investigation of deep energy levels in heterostructures based on GaN by DLTS 8th *Int. Conf. on Advanced Semiconductor Devices and Microsystems* (IEEE) pp 135–8
- [181] Caesar M, Dammann M, Polyakov V, Waltereit P, Bronner W, Baeumler M, Quay R, Mikulla M and Ambacher O 2012 Generation of traps in AlGaN/GaN HEMTs during RF-and DC-stress test 2012 *IEEE Int. Reliability Physics Symp. (IRPS)* (IEEE) p CD.6.1–CD.6.5